Investigating Cellular Viscoelastic Properties with Nanonet Force Microscopy

Haonan Zhang

Thesis submitted to the faculty of the Virginia Polytechnic Institute and State University
in
partial fulfillment of the requirements for the degree of

Master of Science
In
Mechanical Engineering

Amrinder S Nain, Chair
Kevin Sheets
Ling Li
Mark R Paul
Sohan Kale

April 20, 2022

Blacksburg, VA

Keywords: Living Cell Viscoelastic Property, Nanonet, Non-electrospinning, Outside-in cell excitation

Investigating Cellular Viscoelastic Properties with Nanonet Force Microscopy

Haonan Zhang

Academic Abstract:

Determining the mechanical properties of living cells accurately and repeatably is critical to understanding developmental, disease, and repair biology. The cellular environment is composed of fibrous proteins of a mix of diameters organized in random and aligned configurations. In the past two decades, several methods, including modified atomic force microscopy (AFM) and micro-pipette aspiration have been developed to measure cellular viscoelastic properties at single-cell resolution. We inquired if the fibrous environment affected cellular mechanobiology. Using our non-electrospinning Spinneret based Tunable Engineered Parameters (STEP) fiber manufacturing platform, we developed fused nanonets to measure single-cell forces and viscoelasticity. Using computer-controlled probes, we stretched single cells attached to two-fiber and three-fiber systems precisely and recorded the relaxation response of cells. The viscoelastic properties were determined by fitting the data to the standard linear viscoelastic solid model (SLS), which includes a spring (k_0) in parallel with a spring (k_m)-damper (c_m) series. In cases in which cells are seeded on two fibers, we tested hMSCs and BJ-5TA cells, and the viscoelastic components measurements k_0, k_m, and c_m are 26.16 ± 3.38 nN/μm, 5.81 ± 0.81 nN/μm, and 41.15 ± 5.97 nN-s/μm, respectively for hMSCs, while the k0, km, and cm, measurements of BJ-5TA cells are 20.02 ± 2.89 nN/μm, 4.62 ± 0.75 nN/μm, and 45.46 ± 6.00 nN-s/μm respectively. Transitioning to the three-fiber system resulted in an overall increase in native contractility of the cells while allowing us to understand how the viscoelastic response was distributed with an increasing number of fibers. Viscoelastic experiments were done twice. First, we pulled on the outermost fiber similar

to the two-fiber case. The cell was then allowed to rest for two hours, sufficient time to regain its pre-stretching contractility. The cell was then excited by pulling on the middle fiber. The experimental results of cell seeding on three fibers proved that the viscoelastic property measurements depend on the excitation position. Overall, we present new knowledge on the cellular viscoelasticity of cells attached to ECM-mimicking fibers.

Investigating Cellular Viscoelastic Properties with Nanonet Force Microscopy

Haonan Zhang

General Audience Abstract:

Investigating living cell mechanical properties including the viscoelastic properties of single living cell is critical to understanding developmental, disease, and repair biology. With the advancement of micrometer scale technologies, researchers are able to excite individual living cells. Current methods are mostly based on perturbing cells attached to flat 2D surfaces with limited physiological relevance. Since the native environment of cells is fibrous in nature, we inquired if cellular viscoelasticity could be measured of cells attached to suspended fibers. Using our non-electrospinning Spinneret based Tunable Engineered Parameters (STEP) fiber manufacturing platform, we developed fused nanonets to measure single-cell forces and viscoelasticity. Our suspended, aligned nanonet provides a unique way for us to pull on individual living cells using computer-controlled probes. By controlling the aligned fiber spacing, we are able to determine how many fibers the cells were seeded on. We first measured the viscoelastic properties of human mesenchymal stem cells(hMSCs) and human fibroblast BJ-5TA cells seeded on two fibers. The standard linear solid (SLS) model, which includes a spring in parallel with a spring-damper series, was used to quantitatively analyze the viscoelastic properties of cells. By giving the excitation on one fiber and measuring the cell forces on the other fiber, we calculated the corresponding spring constants and damping coefficients of the model. Then we investigated the viscoelastic properties of hMSCs seeded on three fibers by giving the excitation on the outermost fiber and then the middle fiber. Between the two excitations, the cell was allowed to relax for two hours and regain contractility. Our results confirm that the viscoelastic properties measurements depend on the excitation

position. Overall, we present a new fiber-based force measurement system capable of determining the viscoelastic response of cells repeatably.

Table of Contents:

Table of figures:

Introduction:

Closely related to cell migration, proliferation, and many other cell-extracellular matrix (ECM) interactive cell behaviors, viscoelastic properties of living cells and tissues play a crucial role in many of their activities which require their solid-like and viscous-like characteristics[1]. Previous research had shown that the differentiation of individual cell viscoelastic properties highly affects collective cells' behaviors[2]. Therefore, being able to investigate cellular viscoelastic properties is important to understanding not only individual cell behaviors, but also larger scale living systems' behaviors.

Both the cytoskeleton and cytosol contribute to cellular viscoelasticity[3]. Cytoskeletal viscoelasticity can influence cell morphology, motility and division (mitosis)[4], while cytoplasmic viscosity dominating processes of macromolecular movement[5]. Cytoskeletal viscoelasticity is complex since it depends on the properties, structures, and arrangements of its three main components[6][7][8], actin stress fibers[9], intermediate filaments, and microtubules. Although the cellular viscoelasticity is a result of the heterogeneous properties of both cytoskeleton components and cytosol, our understanding of cell viscoelasticity comes mostly from studying each of these elements separately[3][4].

Since individual cell not only shows elastic behaviors, but also performs plastic deformation when external forces are applied to it[10], the mechanical model for cell viscoelastic properties must include both springs (elastic elements) and dampers (plastic elements). However, the Maxwell model (which was established by James Clerk Maxwell) cannot reflect the recovery (strain relaxation) of the cell, while the Kelvin–Voigt model (which is named after the Lord Kelvin and after Woldemar Voigt) lacks the ability to reflect the stress relaxation of the cell. We decided to use the standard linear solid model (SLS, also known as Zener Model, Maxwell representation) for cellular viscoelasticity analysis. (**Figure 1**)

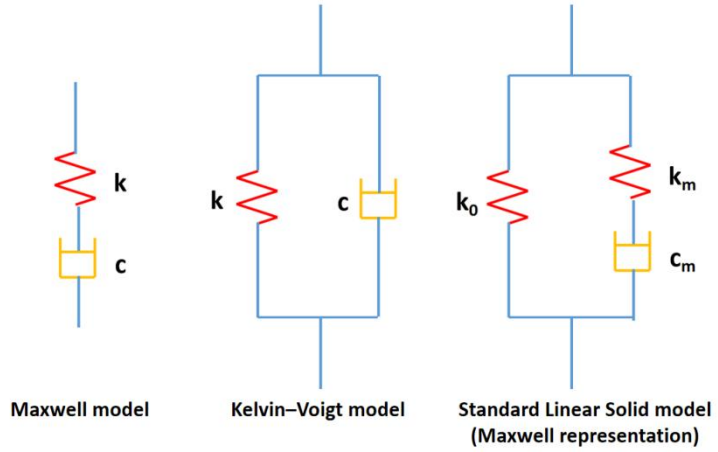

Figure 1. Maxwell model, Kelvin-Voigt model, and Standard Linear Solid model

Investigating the quantitative values of each viscoelastic elements in the model demands the ability to generate excitation to the cell and acquire cell response to that excitation in a nano-Newton scale. Therefore, the ability to accurately generate Outside-In (OI) forces to a cell and acquire Inside-Out (IO) forces of that cell are needed for cell viscoelastic property measurements. To generate OI force excitation to the cells, tools, and techniques including optical traps[11], glass micro-cantilevers[12], atomic force microscopy (AFM)[13], micropipette aspiration[14], and magnetic tweezers[15] had been developed. Wrinkling membranes[16], traction force microscopy[17], and micropillars[18] have been used to study the IO forces.

The modification of these tools provides the ability to generate excitation and measure the cell response spontaneously which makes acquiring cellular viscoelastic properties possible (**Table 1**).

Project	Author	Cell Type	Extracellular Matrix Type	Drug Treatment	Mechanical Model	Excitation Method
Measuring Viscoelastic Properties of Living Cells	Yang Bu, Long Li, Chendong Yang, Rui Li, Jizeng Wang	human normal liver (L02), hepatic cancer (HepG2), hepatic stellate (LX2) and gastric cancer (NCI-N87), human normal gastric (GES-1) and gastric cancer (SGC7901) cells	Flat, 35-mm petri dishes	None	incompressible linear viscoelastic solids	Atomic force microscopy (AFM)
An AFM-Based Stiffness Clamp for Dynamic Control of Rigidity	Kevin D. Webster, Ailey Crow, Daniel A. Fletcher	NIH 3T3 fibroblast cells	Flat, KOH cleaned glass substrates	None	Standard linear solid model (SLS, Maxwell representation)	Modified Atomic force microscopy (AFM)
Viscoelastic behaviour of human mesenchymal stem cells	Samuel CW Tan, Wen X Pan, Gang Ma, Ning Cai, Kam W Leong and Kin Liao	Human mesenchymal stem cells (hMSCs)	Flat, glass coverslip (0.17 mm thick)	cytochalasin D with different concentrations	Standard linear solid model (SLS, Maxwell representation)	Micropipette aspiration
The role of the cytoskeleton in the viscoelastic properties of human articular chondrocytes	Wendy R. Trickey, T. Parker Vail, Farshid Guilak	Human articular chondrocytes	A chamber with flat surfaces	Cytoclialasin D, Acrylrmide, and Colchicinc with different concentrations	Standard linear solid model (SLS, Maxwell representation)	Micropipette aspiration
Investigating Cellular Viscoelastic Properties with Nanonet Force Microscopy	Haonan Zhang, Amrinder Nain	Human mesenchymal stem cells (hMSCs)	Suspended gused-fiber nanonet	None	Standard linear solid model (SLS, Maxwell representation)	Glass micropipette pulling on Nanonet force microscopy (NFM)

Table 1. Methods for cell viscoelasticity measurements.

AFM is widely used in force related cell biology research. By assuming living cells as incompressible linear viscoelastic solids, mathematical equations can be derived, and computational results can be compared to real cell force measurements to determine if the living cells can be treated as linear viscoelastic material[19]. With a modified AFM, the apparent cantilever stiffness can be adjusted, and the spring constants and damping coefficients can be determined based on SLS model[20] (**Figure 2**). However, AFM based methods require living cells to be seeded on flat 2D surfaces which is not the common ECM where many cell types inhibit.

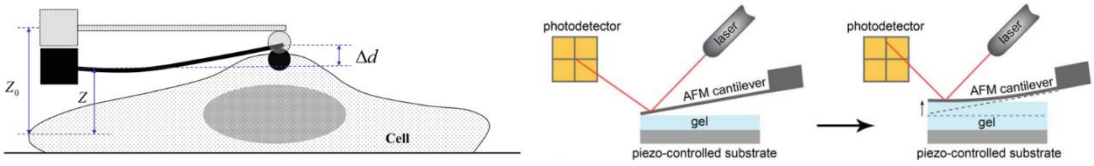

Figure 2. Using AFM[19] and modified AFM for flexible apparent cantilever stiffness[20] to measure cellular viscoelastic properties.

Micropipette aspiration method do provide another way to acquire cellular viscoelastic property. By recording the cell aspiration length into the micropipette and applying SLS model, the cellular viscoelasticity can be determined[21]. Although cells suspended in a chamber can better mimic suspended ECM where many cell types inhibit[6], [22] (**Figure 3**), the chamber surfaces still fail to mimic the fibrous ECM which could

significantly affect the cell-ECM adhesion. Also, a living cell is considered to be a heterogenous body instead of a homogeneous material, which indicates that measurements taken using micropipette aspiration method may not reflect the cellular viscoelasticity of the whole cell body.

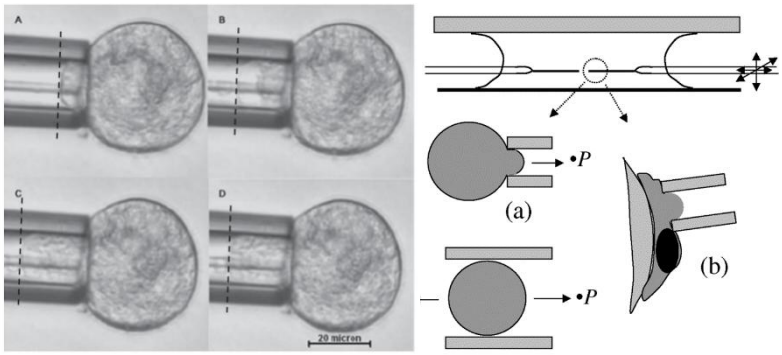

Figure 3. Using micropipette aspiration methods to measure cellular viscoelastic properties[21], [22].

The natural cellular environment is fibrous, termed extracellular matrix (ECM) composed of fibrous proteins with a mix of diameters (nano-micro) and deposited in a variety of orientations (random-aligned) in multiple architectures (sparse-dense multilayer). Previous research has shown that the properties of ECM (including fiber density, fiber diameter, fiber orientation, and other physical properties) would affect not only cellular migration mode, but also the migration behavior of cell collectives[23] (**Figure 4**).

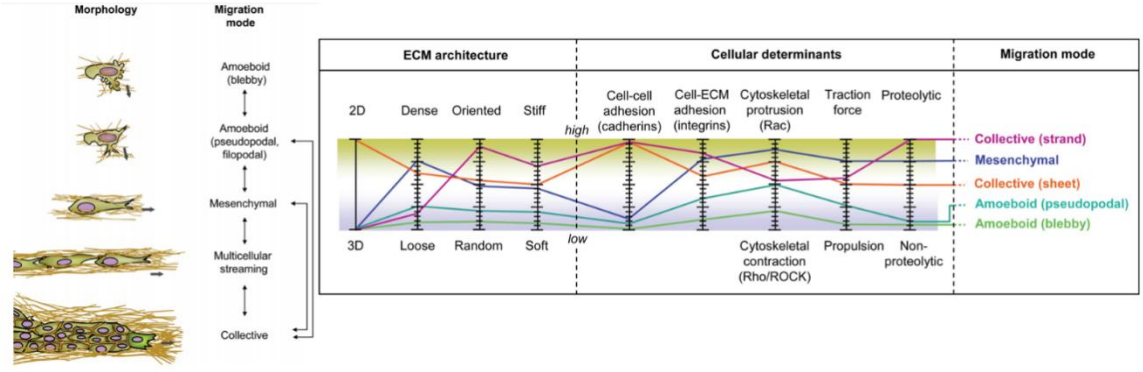

Figure 4. Morphology of ECM would affect cell migration modes[23].

In vivo, the tissue architecture varies considerably with a mix of fiber diameters and pore sizes [23]–[26]. When the pore size of the fibrous ECM is large, cells may only attach to several fibers. The pore size of ECM will also affect cell migration behaviors which indicates that fiber net morphology can affect cell migration speed[26] (**Figure 5**).

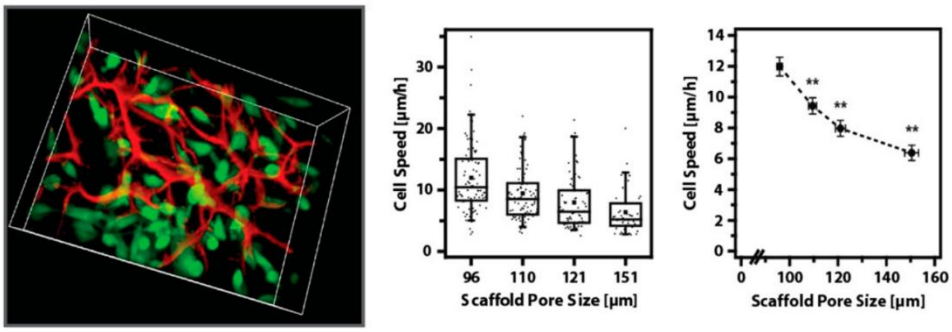

Figure 5. Three-dimensional confocal micrograph of the porous microstructure of a CG scaffold (red) seeded with labeled NR6 cells (green). Pore sizes of the ECM can affect cell migration speed[26].

To better mimic the suspended fibrous ECM, we developed nanonet force microscopy (NFM) based on non-electrospinning Spinneret based Tunable Engineered Parameters (STEP) technique which allowed us to create suspended fibrous ECM[27], [28] (**Figure 6**).

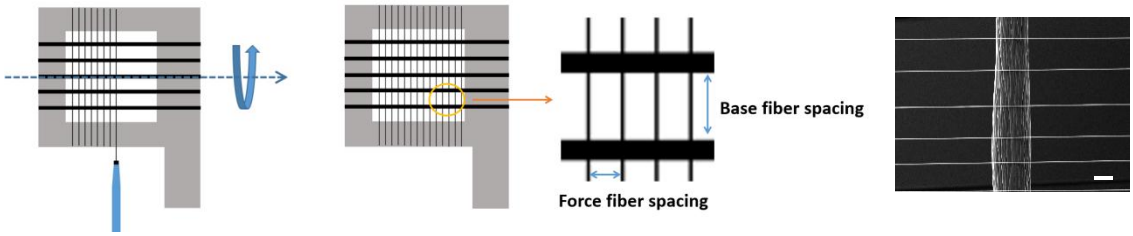

Figure 6. Non-electrospinning Spinneret based Tunable Engineered Parameters (STEP) technique (scale bar: 10 µm).

Recently, intravital imaging of breast cancer cells showed the ability of cells to contact individual collagen fibers and exert forces resulting in their deformation, matching our findings of cell protrusions applying forces on suspended fiber systems[29], [30]. As

shown in **Figure 7**, the timepoint insets (yellow box) highlight cells contacting and displacing collagen fiber. Arrowhead(yellow) indicates point of contact and deformation. This phenomenon matches the "perpendicular lateral protrusions" we observed with cells seeded on STEP fibers. This indicates that cells seeded on STEP fiber nets show similar behaviors as cells in 3D fibrous ECM and 1D micropattern did.

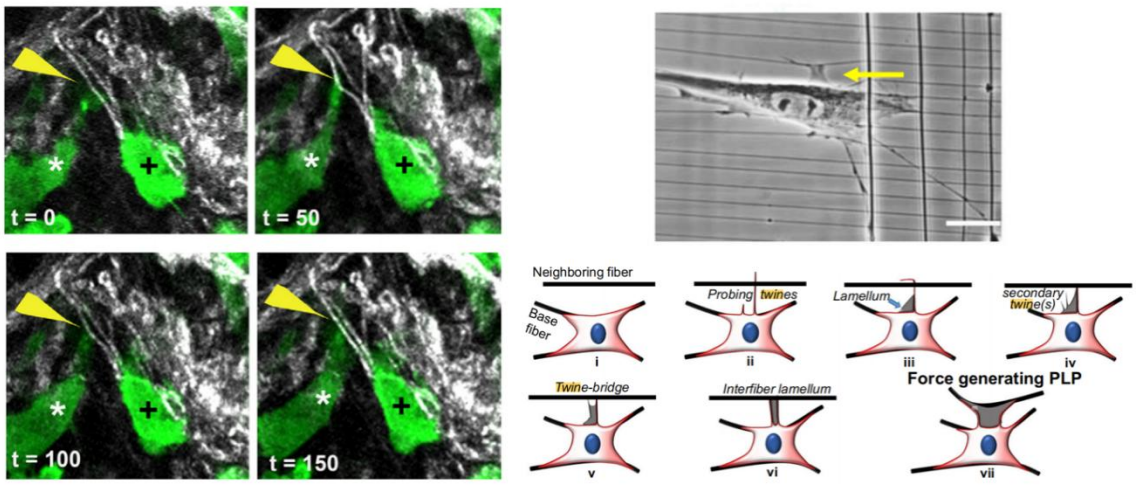

Figure 7. Image from a living GFP-LifeAct-MDA-MB-231 tumor in the mammary fat pad[30] and perpendicular lateral protrusions[29].

Furthermore, using suspended fiber networks, we have shown that the migratory modes match the findings from 3D cell-derived matrices and 1D fibrillar lines (commonly used to study 3D migration)[23], [31]. Cells on 3D cell-derived matrices have high migration persistence which is very different to cells on 2D flat surfaces. However, this high migration persistence was also observed on cells seeded on 1D micropatterns and high-density STEP crosshatch fibers. Again, this phenomenon indicates that cells spread on suspended fibrous STEP fibers show similar behaviors as cells in 3D ECM. Thus, through different studies, we have shown that suspended fibers mimic in vivo fibrous characteristics and have physiological relevance.

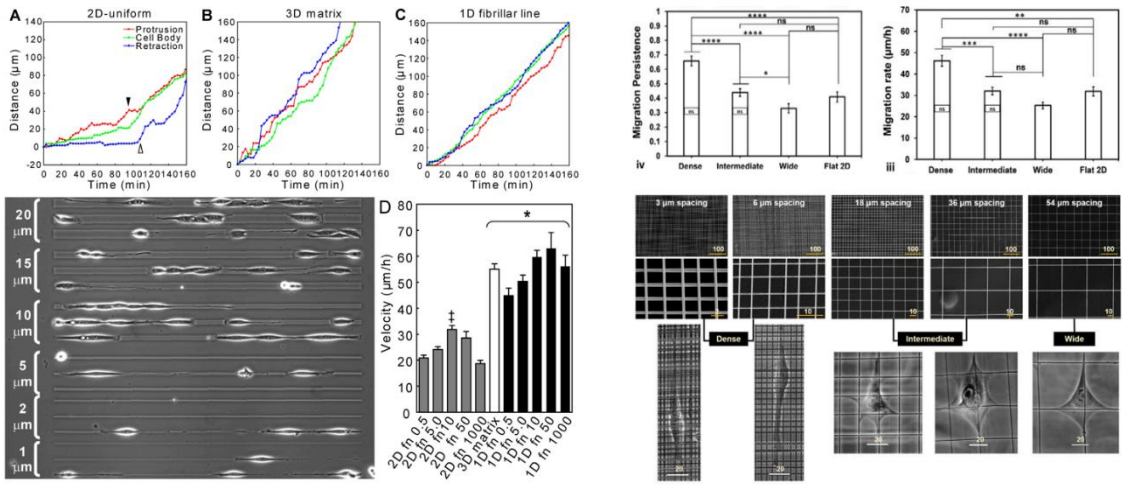

Figure 8. Cell migration behaviors are similar in 3D fibrillar extracellular matrix (ECM) and on 1D fibrillar patterns[23], and it is similar to cell migration behaviors on high density crosshatch STEP fibers[31].

Nanonet Force Microscopy (NFM) was developed based on STEP fibers in our lab[27], [28], [31], [32]. We could generate OI excitation to individual living cells seeded on suspended ECM by pulling fibers of the ECM with computer-controlled micro-pipettes. This technique provides us the ability to exert external forces on cells by deforming living cells without directly touching the cell or disrupting the cell-ECM adhesion. Similarly, we can observe, and record cell IO forces using an optical microscope and monitor cell responses to the OI excitation with respect to time.

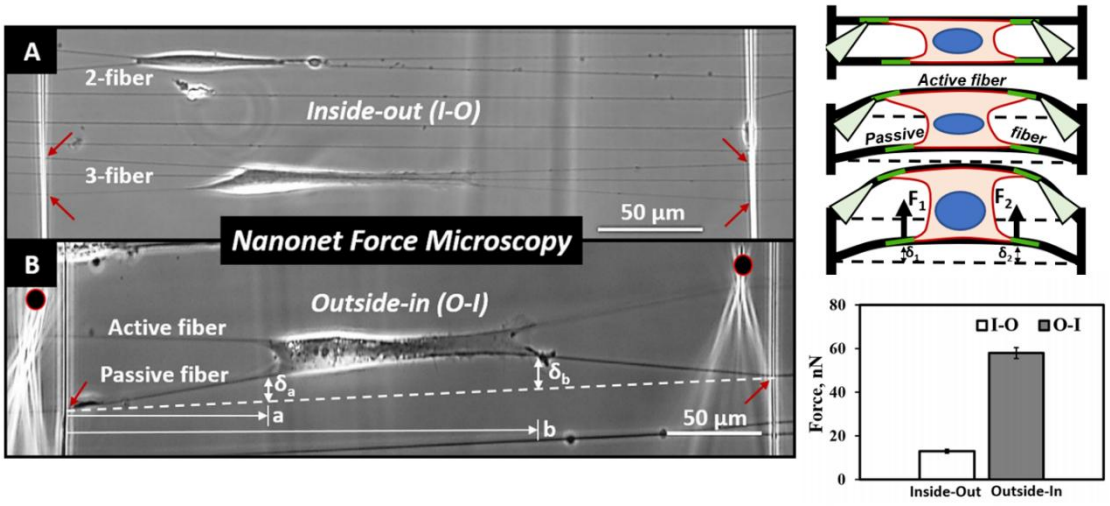

Figure 9. NFM is capable of generation outside-in (OI) excitation and measuring inside-out cell force[31].

With the NFM developed in our previous work, we are able to investigate cell viscoelastic properties by generating a step excitation to living cells and recording the cell bodies' relaxation process. The step excitation can be created by pulling ECM fibers with fast speed, while the cell body relaxation can be monitored by interpreting ECM fiber deformation to cell IO forces. Using the standard linear solid model (SLS), we could evaluate the spring constant and damping coefficient of a living cell body. The mechanical values solved using the SLS can be further interpreted to quantitative properties with physical meanings. By changing the morphology of the ECM, we can further expand the potential of our system. Analyzing cells with a variety of varied sizes or increasing the complexity by pulling cells seeded on multiple fibers may be achieved by making fibrous ECM with higher nanonet densities or smaller fiber diameters.

Methods:

Cell Culturing:

Human Mesenchymal Stem Cells (hMSCs) were purchased from Lonza (Basel, Switzerland) at passage 2. The hTERT-immortalized foreskin fibroblast cell line (BJ-5TA) were purchased from ATCC (Manassas, VA, USA) at passage 2. The cells were maintained in Mesenchymal Stem Cell Growth Medium (MSCGM) purchased from Lonza (Basel, Switzerland) at 5% CO^2, 37 ^oC incubator in T25 (Corning, USA) and T75 cell culture flasks (Corning, USA). The following steps were performed to seed the cells on the STEP nanonet scaffold. First, the cell medium was aspirated out of the cell culturing flasks, PBS (Corning, USA) was used to rinse the cells twice, and the cells were incubated at 5% CO^2 and 37 ^oC with 600 µL (1800 µL for cells in T75) of Trypsin/EDTA for MSC (Lonza, Switzerland).Second, the cells were re-suspended in fresh MSCGM (Lonza, Switzerland) and seeded on the top of fibronectin coated nanonet scaffolds. The cells can either be seeded on two or three fibers depending on the fiber spacing and cell size. (**Figure 10**)

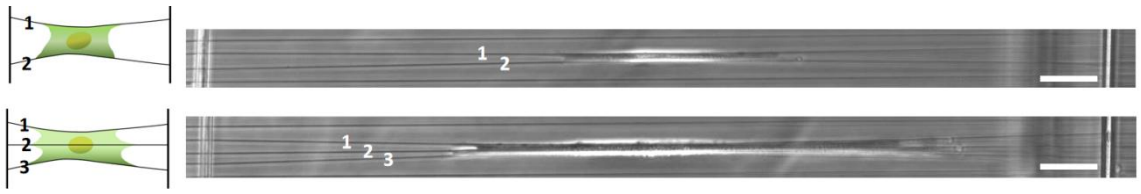

Figure 10. Cell seeded on two or three fibers.

Third, the wells containing the scaffolds and the seeded cells were incubated at 5% CO^2 and 37 ^oC for one hour after the seeding, and 2 mL of fresh MSCGM (Lonza, Switzerland) was added to the well with 1% pen strep (Gibco, USA) and 15 mM HEPES (Gibco, USA).

Imaging:

After the cells were attached to and fully spread on the nanonet, the time-lapse videos were taken at 1 frame per second using Zeiss AxioObserver Z1 (Zeiss, Thornwood, NY), which is a microscope with incubating capacity. An AxioCam mRm camera along with 10 X phase objectives were used for imaging. Videos were processed using ZEN 3.4 blue edition (Zeiss, Thornwood, NY) and imageJ (National Institutes of Health, USA) for further analysis. The fiber deflections and cell forces were analyzed using MATLAB Code developed previously in STEP Lab.

Nanonet Fiber Spinning:

Polystyrene (PS) (Scientific Polymer Products, Ontario, NY) with molar weight of 1.5×10^7 g mol^{-1} (for base fibers) and 2.5×10^6 g mol^{-1} (for force fibers) were dissolved in xylene (Carolina Biological Supply, NC) at 5% (for base fibers) and 9% (for force fibers) to make fiber spinning solutions. Metal substrate with 4mm × 4mm hollow frames were prepared. The metal scaffolds were fixed on the STEP platform and rotated at 6 (both for base fibers and force fibers) or 10 (only for force fibers) rounds per second. Suspended and aligned PS nanofibers were attached to rotating metal scaffolds at room temperature. A combination of 9%, 2.5×10^6 g-mol^{-1} PS solution and 6 round per second substrate rotational speed yields force fibers with 500 nm diameter; 5%, 2.5×10^6 g-mol^{-1} PS solution and 10 round per second substrate rotational speed yields force fibers with 200 nm diameter; and 5%, 1.5×10^7 g mol^{-1} PS solution and 6 round per second substrate rotational speed yields base fibers with more than 2 micrometers diameter. By controlling the horizontal (Figure 1) movement speed of the scaffolds, the force fiber spacing are controlled to be 10 micrometers, 15 micrometers, or 20 micrometers depending on the usage of the nanonet. The nodes where the force fibers and base fibers intercepts are fused to form STEP nanonets with clamped boundary conditions by using a custom solvent evaporation-based fusing method.

The scaffolds with nanonet were attached to the glass bottom of the single well plate (Cellvis, Canada) using high vacuum grease (Dow Corning, Midland, MI), and sterilized

with 70% ethanol for 10 minutes in a sterile hood. After the scaffolds are sterilized, the ethanol was aspirated out and rinsed with phosphate buffered saline (PBS), Corning, USA) twice. The fibers were coated with fibronectin from bovine plasma (8 μg-ml^{-1}, Sigma- Aldrich, St. Louis, MO) for more than one hour while incubated at 5% CO^2 and 37 ^oC.

Glass Probe Design and 2-Fiber Case Pulling:

P-1000 Flaming/Brown micropipette puller (Sutter Instrument, Novato, CA) was used to reduce the 1.0-mm-diameter capillary glass rods (Sutter Instrument) to 1-μm-diameter glass probes. The scaffold with nanonet was pulled by a pair of glass probs controlled by a computer-controlled MP-285 motorized manipulator (Sutter Instrument) (**Figure 11**). The pulling direction is always pointing outward from the cell. The programmed pulling speed is 35 μm/s to mimic a step force excitation, while the pulling distance is around 50 μm.

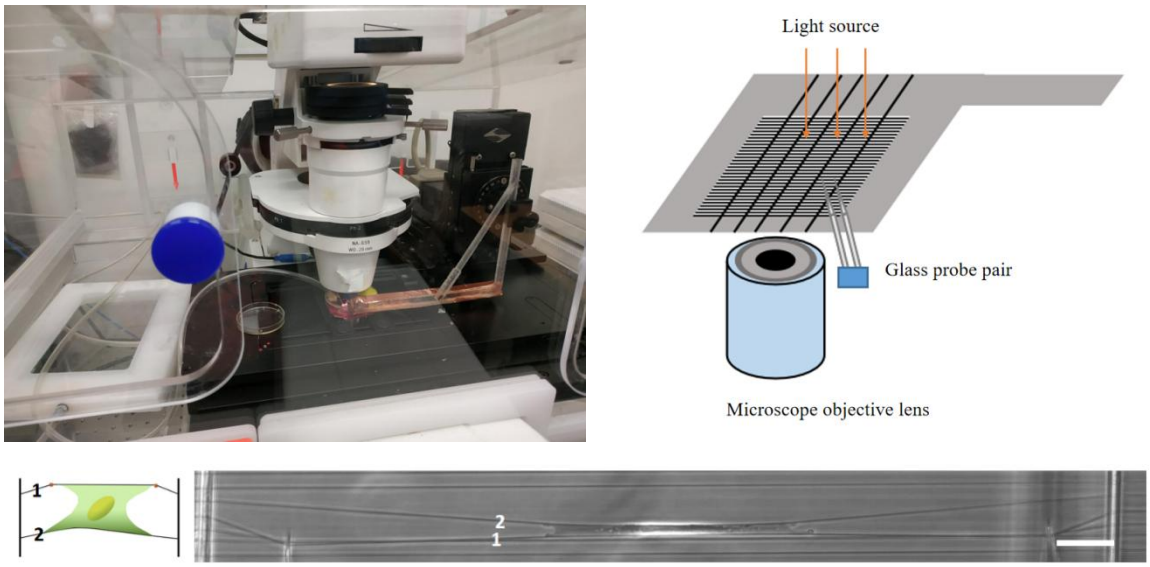

Figure 11. Setup of the fiber pulling system and an example of cell pulling image.

For cells attach to 2 parallel fibers, we create excitation by pulling one of the fibers (excitation fiber) in the outward direction and record the response of the other fiber (responding fiber). The excitation fiber and the responding fiber are marked as fiber 1

and fiber 2 in **Figure 11**. After the step excitation, the responding fiber reaches its maximum deformation followed by a deformation relaxation process until it reaches steady state. (**Figure 12**)

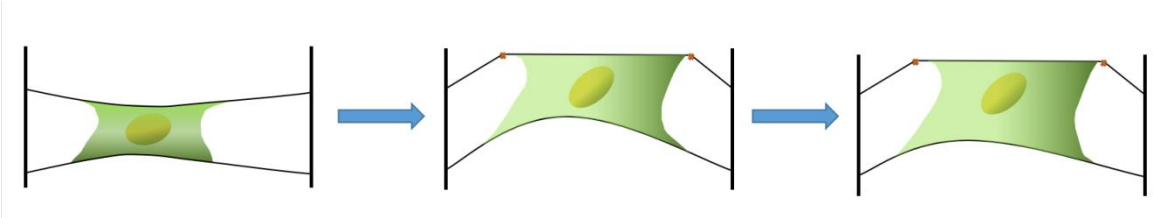

Figure 12. 2-fiber case cell pulling and relaxation

The deformation recovery speed reduces as the responding fiber recovers to steady state position. Images were taken every 3 seconds for a minute to record the fiber relaxation for later cell force measurements.

3-Fiber Case Pulling:

We did two groups (group A and group B) of experiments with cells spread on 3 parallel fibers. In group A experiments, the excitation was given through one of the side fibers with outward direction followed by a second pulling on the same fiber with the same direction. First and second pulling were separated by 2 hours to allow cell body recovery (**Figure 13**). For both the first pulling and second pulling, images were taken every 3 seconds for a minute to record the two responding fibers' (middle fiber and side fiber shown in **Figure 13**) deformation for later cell force measurements.

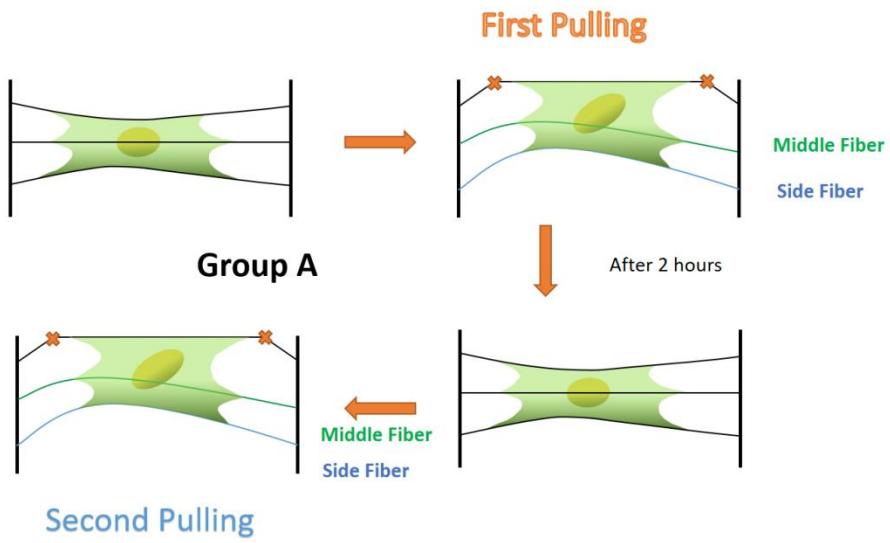

Figure 13. 3-fiber case group A experiment procedures

In group B experiments, the excitation was given through one of the side fibers with outward direction followed by a second pulling on the middle fiber with the same direction. Similar to group A experiments, first and second pulling were separated by 2 hours to allow cell body recovery. (**Figure 14**) For both the first pulling and second pulling, images were taken every 3 seconds for a minute. For the first round of pulling, we recorded the two responding fibers' (side fiber and middle fiber shown in **Figure 14**) deformation for later cell force measurements. However, for the second round of pulling, only one responding fiber (side fiber shown in **Figure 14**) deformation was recorded for later cell force measurements.

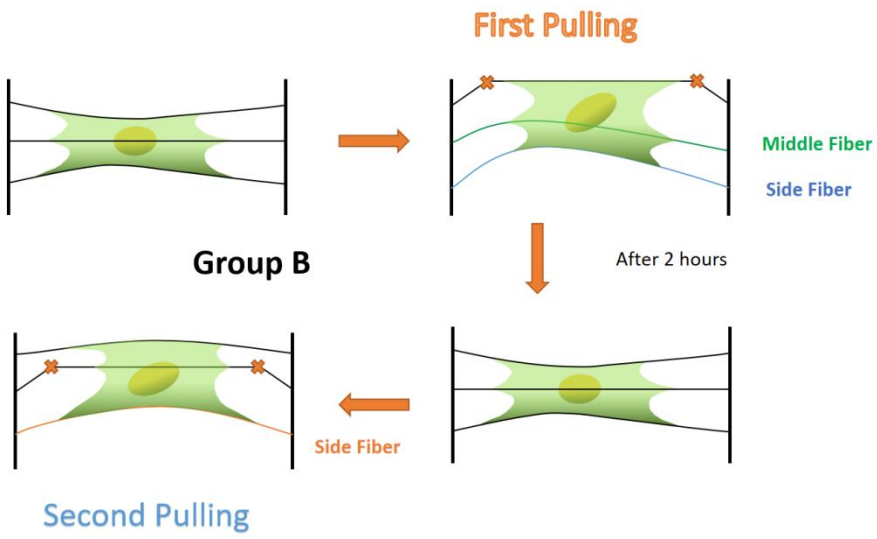

Figure 14. 3-fiber case group B experiment procedures

Cell Viscoelastic Property Calculation:

Standard Linear Solid Model (SLS) was used to quantitatively measuring cell viscoelastic properties (**Figure 15**).

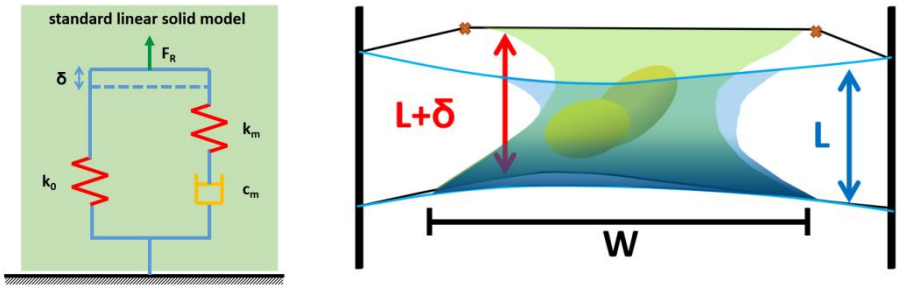

Figure 15. Standard linear solid model (SLS) and cell pulling

The governing equation of SLS when the modeling body experiences a step force excitation is listed in equation 1.

$$F = F_0 + F_m \cdot e^{-\frac{k_m}{c_m}t} \quad (1)$$

Where F is the total force experienced by the cell body. F_0 is the force experienced by the spring k_0, F_m is the force on the spring-damper series part (spring k_m and damper c_m) of the model right after the step excitation, k_0, k_m, and c_m represent the spring constants and damping coefficients of the mechanical components of the model respectively, and t is the time after the step force excitation.

Since cell relaxation length is neglectable compared to the cell deformation, we assume that the cell body deformation (δ) is constant during the cell relaxation process. With this assumption, we are able to rewrite equation 1 with cell deformation δ (equation 2).

$$F = \delta \cdot (k_0 + k_m) \cdot e^{-\frac{k_m}{c_m} t} \quad (2)$$

Where δ is the cell deformation after the step force excitation.

To determine the values of k_0, k_m, and c_m, we need to measure the cell deformation δ and record total force F experienced by the cell body with respect to time. Cell deformation can be determined by direct measurements from the images. The cell forces are measured with nanonet force microscopy (NFM) previously developed by our team[27]. Cell force measurements were taken every 3 seconds, and 15 force measurements were taken for each cell pulling case (**Figure 16**).

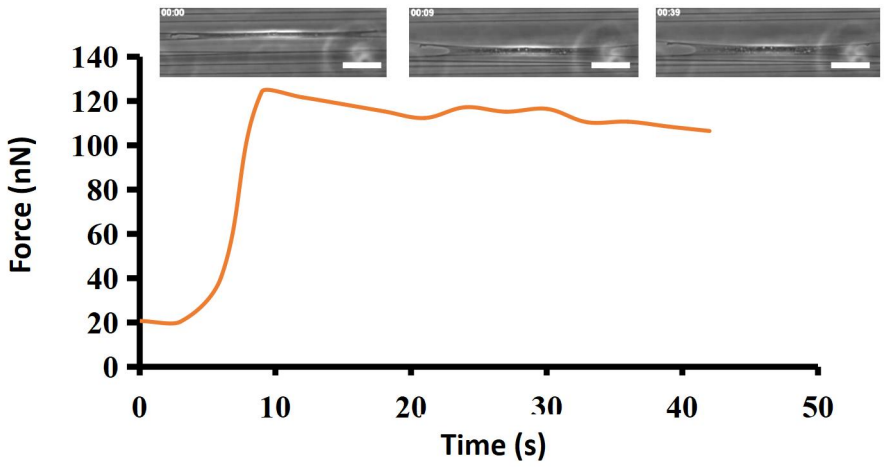

Figure 16. An example of cell force relaxation after the step force excitation (2-fiber case)

The average value of the last 5 force measurements was used as the steady state force (F_0) for each case. The value of k_0 can be determined with known steady state force (F_0) and cell deformation (δ). Then the force measurements after the step force excitation were fitted to an exponential function using MATLAB curve fitting tool (MATLAB ver. R2017a, USA) to determine the values of k_m and c_m based on the fitting curve equations ($R^2 > 0.7$ for all cases analyzed). (**Figure 17**)

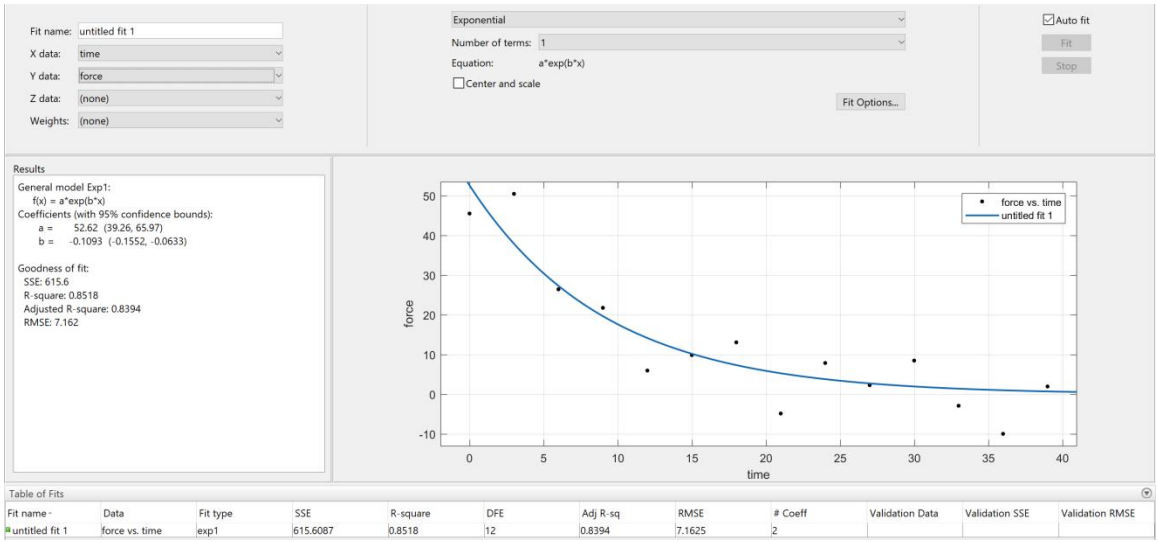

Figure 17. An example of exponential curve fitting of the cell force relaxation

Middle Fiber Force Measurements:

The force on the middle fiber (shown in **Figure 13** and **Figure 14**) in 3-fiber case cell pulling experiments were measured with nanonet force microscopy (NFM) previously developed by our team[27] before the excitation was given. For each round of the 3-fiber case cell pulling, one force measurement was recorded.

Immunohistochemistry and immunofluorescence imaging:

Scaffolds containing hMSCs or BJ-5TA cells were fixed using 4% paraformaldehyde (PFA) and permeabilized in 0.1% Triton X100 solution. Then the cells were blocked in 10% goat serum (Seracare, Milford, MA, USA). Primary rabbit anti-paxillin antibodies (Invitrogen, Waltham, MA, USA) and secondary goat anti-rabbit Alexa Fluor 488

(Invitrogen) antibodies were diluted 1:100 and incubated for 12 h at 4 ºC and 45 min at room temperature protected from light respectively. Nuclei were counterstained with DAPI (Invitrogen) and actin was counterstained with Rhodamine Phalloidin (Invitrogen). During imaging, scaffolds with fixed cells were kept hydrated in 2 mL of PBS. Fluorescent images were taken with the Axio Observer Z1 microscope (Zeiss).

Cell Spreading Area Measurements:

The nucleus and cell body areas of cells spread on nanonet were measured based on fluorescence images for 50 hMSCs and BJ-5TA cells using ImageJ (National Institutes of Health). The nucleus to cell area ratio was calculated:

$$R = \frac{A_{nucleus}}{A_{cell-body}} \quad (3)$$

Where R is the nucleus to cell area ratio, $A_{nucleus}$ and $A_{cell\text{-}body}$ are area measurements of cell nucleus and cell body in μm^2.

For 2-fiber case cell pulling experiments, the cell body area before and right after the step force excitation was measured from phase images recorded during cell pulling experiments using ImageJ (National Institutes of Health). For 3-fiber case cell pulling experiments, the cell body area of the two sections separated by the middle fiber (shown in **Figure 13** and **Figure 14**) before and after the step force excitation was measured using ImageJ (National Institutes of Health).

The area increase after the excitation was calculated:

$$\Delta A = A_{after} - A_{before} \quad (4)$$

Where ΔA is the area increase after the excitation, A_{after} and A_{before} are area measurements of cell body or cell body sections after and before the excitation in μm^2.

Statistical Analysis

Sample populations were tested for statistical significance using Student's

t-test in the software MATLAB (MATLAB ver. R2017a, USA) to determine significant differences. Values are reported as mean ± 1 SE.

In all box plots, "X" marks individual data point, "O" marks the average value. 25th percentile (Q1), median (Q2), and 75th percentile (Q3) is included in the interquartile range (IQR). The "minimum" and "maximum" represents the values of $Q1 - 1.5IQR$ and $Q3 + 1.5IQR$ respectively.

Results and Discussion:

Two-Fiber Case Cell Pulling:

When cells spread on two fibers, pulling the excitation fiber (fiber 1 in **Figure 11**) would cause a rapid increase of the responding fiber force (fiber 2 in **Figure 11**). This fiber force shows exponential decay after it reaches its maximum value, which matches the expectation of the standard linear solid model (SLS). Since hMSCs is much larger in size and can exert much larger forces to the extracellular matrix (ECM) compared to BJ-5TA cells, the maximum responding fiber force of hMSCs (153.67 ± 18.13 nN) cases is also larger compared to those responding fiber force of BJ-5TA cell cases (111.39 ± 8.82 nN). We then calculated the corresponding spring constants and damping coefficients values of hMSCs and BJ-5TA based on the SLS. (**Figure 18**)

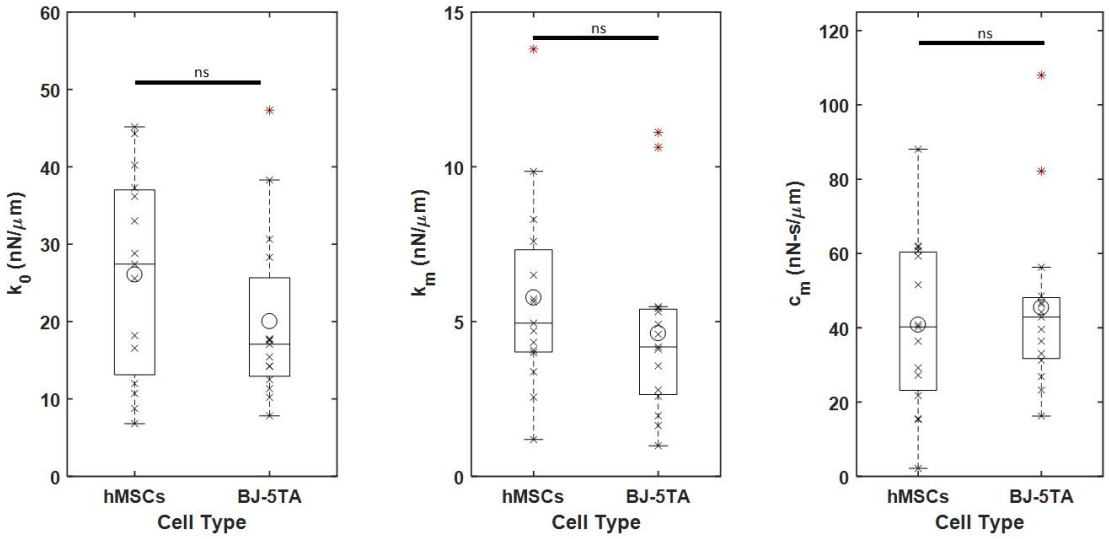

Figure 18. Spring constants and damping coefficients of hMSCs and BJ-5TA cells based on SLS model (n = 15).

Surprisingly, there is no significant difference between the spring constants and damping coefficients values of hMSCs and BJ-5TA despite of their different cell sizes (**Appendix E**), different nucleus to cell area ratio (**Figure 19**, hMSCs (12% ± 0.5%) and BJ-5TA

cells (18.5% ± 0.7%)), and different cell forces. The k_0, k_m, and c_m, measurements of hMSCs are 26.16 ± 3.38 nN/µm, 5.81 ± 0.81 nN/µm, and 41.15 ± 5.97 nN-s/µm respectively, while the k_0, k_m, and c_m, measurements of BJ-5TA cells are 20.02 ± 2.89 nN/µm, 4.62 ± 0.75 nN/µm, and 45.46 ± 6.00 nN-s/µm respectively. There is no clear correlation between the cell area change (before and right after the cell pulling) and the viscoelastic properties calculated for both hMSCs and BJ-5TA cells (**Figure 19**). These results confirm that the viscoelastic properties measured using our system will not be affected by the magnitude of the step force excitation.

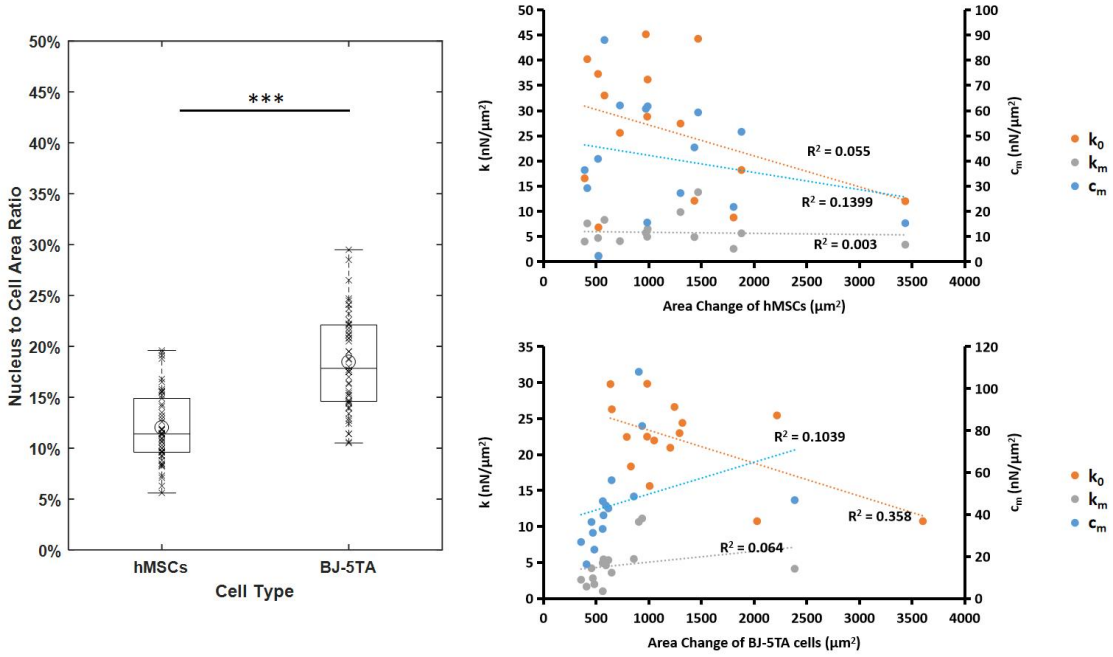

Figure 19. Nucleus to cell area ratio (n = 50) and area change during the cell pulling vs. viscoelastic properties for 2-fiber case cell pulling experiments.

To better understand the viscoelastic properties of the cells, we converted the spring constants and damping coefficients to properties that can eliminate the effects of cell shape and size. We have converted the spring constants and damping coefficients calculated based on SLS to properties with the same unit as young's modulus and dynamic viscosity using a customized method (**Appendix F**).

Although the conversion did not provide the young's modulus nor the dynamic viscosity of the cell body directly (we call them modified stiffness and viscosity), it did provide a better way to compare the cell body properties of different cell types. The modified stiffness of both cell types is similar. The cell body stiffness is mainly determined by cytoskeleton elements including actin filaments, microtubules, and intermediate filaments. Since the composition and structure of cytoskeleton of hMSCs and BJ-5TA are similar, it is reasonable that the modified stiffness of these two cell types is similar. However, the modified viscosity measurements are significantly different between these two cell types. (**Figure 20**)

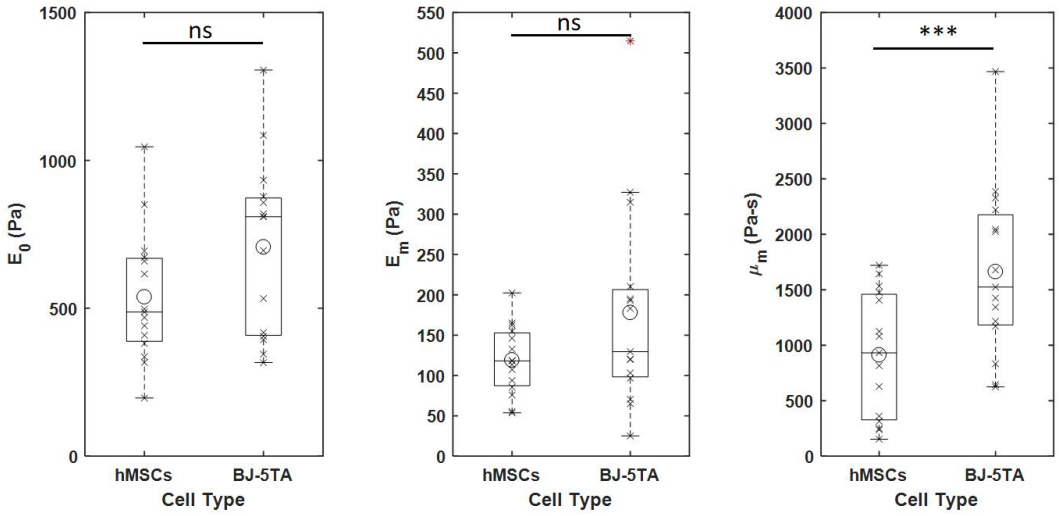

Figure 20. The modified stiffness and viscosity of hMSCs and BJ-5TA. (n = 15)

This may be the result of different cell size (nucleus to cell area ratio) and cell organelle properties.

Three-Fiber Case Cell Pulling:

Cells spread on multiple fibers when the fiber density of the nanonet is high (small fiber spacing). When a cell spreads on three parallel fibers, the cell body was segmented into two parts by the middle fiber. In this 3-fiber case, the cell forces exerted on the middle

fiber before the excitation is given are small enough for us to ignore the cell orientation (first pulling: 5.6 ± 1.0 nN, second pulling 8.1 ± 1.2 nN) (**Figure 21**).

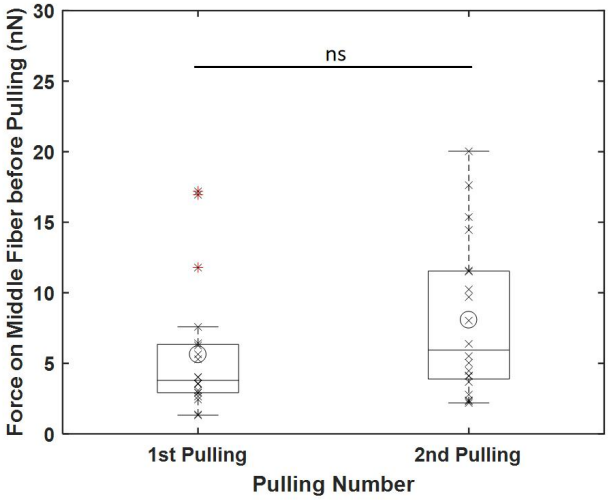

Figure 21. Force on middle fibers before the excitation is given (n = 20).

Thus, the direction in which the step force excitation is given does not affect the measurements of cell viscoelastic properties. It is important for us to answer the following question: can these two parts of the cell be treated as two SLS models in series (**Figure 22**)?

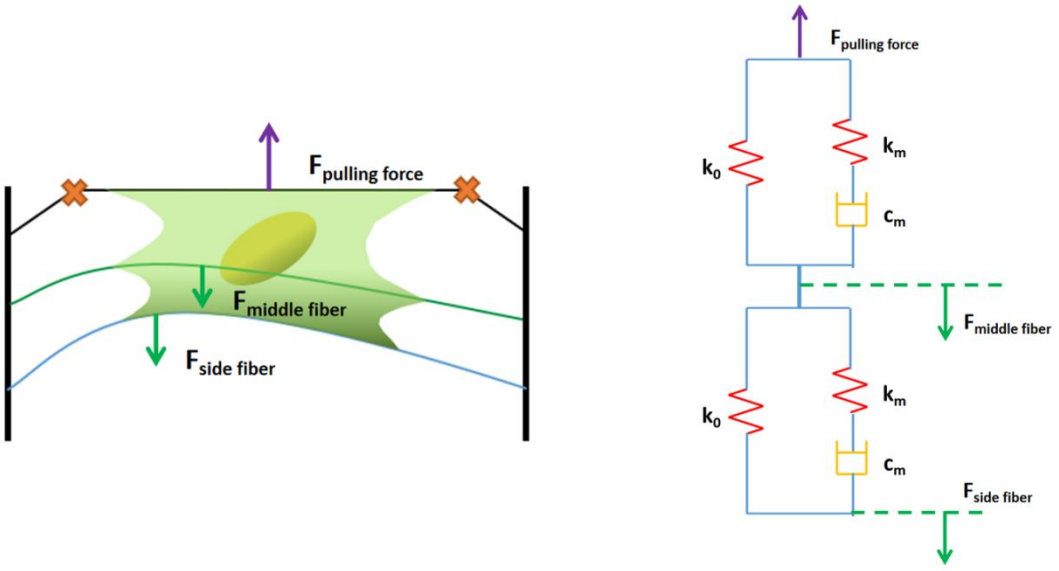

Figure 22. Modify the 3-fiber case cell as 2 SLS model in series.

To answer this question, we did two groups of 3-fiber cell pulling experiments (group A and group B shown in **Figure 13** and **Figure 14**). In group A experiments, for the first pulling, the middle fiber force measurements yield k_0 = 21.90 ± 1.53 nN/μm, k_m = 5.64 ± 0.72 nN/μm, and c_m = 47.82 ± 6.74 nN-s/μm. The side fiber force measurements yield k_0 = 153.54 ± 16.19 nN/μm, k_m = 47.94 ± 11.55 nN/μm, and c_m = 387.97 ± 100.33 nN-s/μm. The second pulling also yields similar results as group A first pulling. The middle fiber force measurements yield k_0 = 18.33 ± 1.54 nN/μm, k_m = 6.32 ± 0.82 nN/μm, and c_m = 49.59 ± 5.32 nN-s/μm. The side fiber force measurements yield k_0 = 158.50 ± 17.57 nN/μm, k_m = 54.91 ± 12.45 nN/μm, and c_m = 447.14 ± 89.67 nN-s/μm. (**Figure 23**) Similar to the measurements in 2-fiber cases, there is no clear correlation between the cell area change (before and right after the cell pulling) and the viscoelastic properties calculated (**Appendix B and Appendix C**).

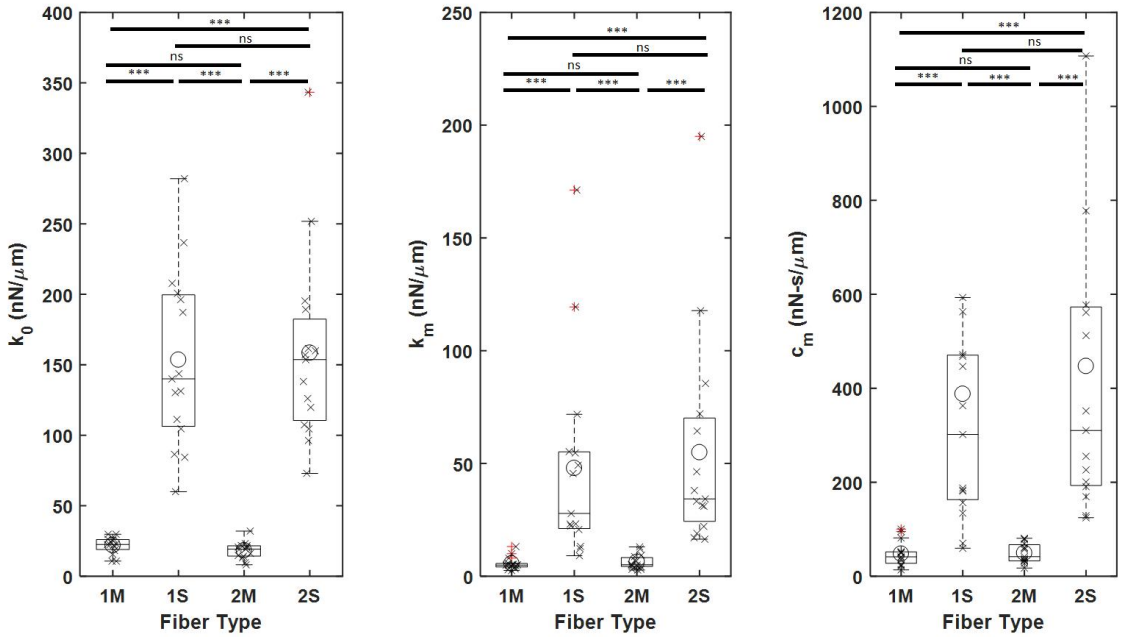

Figure 23. Spring constants and damping coefficients measurements of hMSCs of experiment group A based on forces measurements from first pulling, middle fiber (1M), first pulling, side fiber (1S), second pulling, middle fiber (2M), second pulling, side fiber (2S) (n = 15).

Similar measurements of the first and second pulling indicate that the cell viscoelastic properties did recover. However, the results show that the cell viscoelastic properties measurements based on side fiber (1S and 2S) measurements are significantly larger than those based on the middle fiber (1M and 2M) measurements from both rounds of pulling. This difference is unexpected and indicates that the viscoelastic properties measurements depend on the excitation position, and two parts of the cell cannot be treated as two SLS models in series.

To further understand how the excitation position can affect the cell viscoelastic property measurements, we provide excitations at different positions in group B experiments. Just as expected, the first pulling yields the same viscoelastic property measurements as group A. The middle fiber force measurements yield k_0 = 12.93 ± 0.97 nN/µm, k_m = 4.42 ± 0.49 nN/µm, and c_m = 38.26 ± 3.73 nN-s/µm. The side fiber force measurements yield k_0 = 114.48 ± 17.76 nN/µm, k_m = 34.05 ± 5.48 nN/µm, and c_m = 279.09 ± 38.53 nN-s/µm.

For the second pulling, since the excitation is on the middle fiber, only side fiber measurements can be collected yield k_0 = 20.16 ± 2.24 nN/µm, k_m = 4.87 ± 0.95 nN/µm, and c_m = 40.09 ± 6.19 nN-s/µm (**Figure 24**).

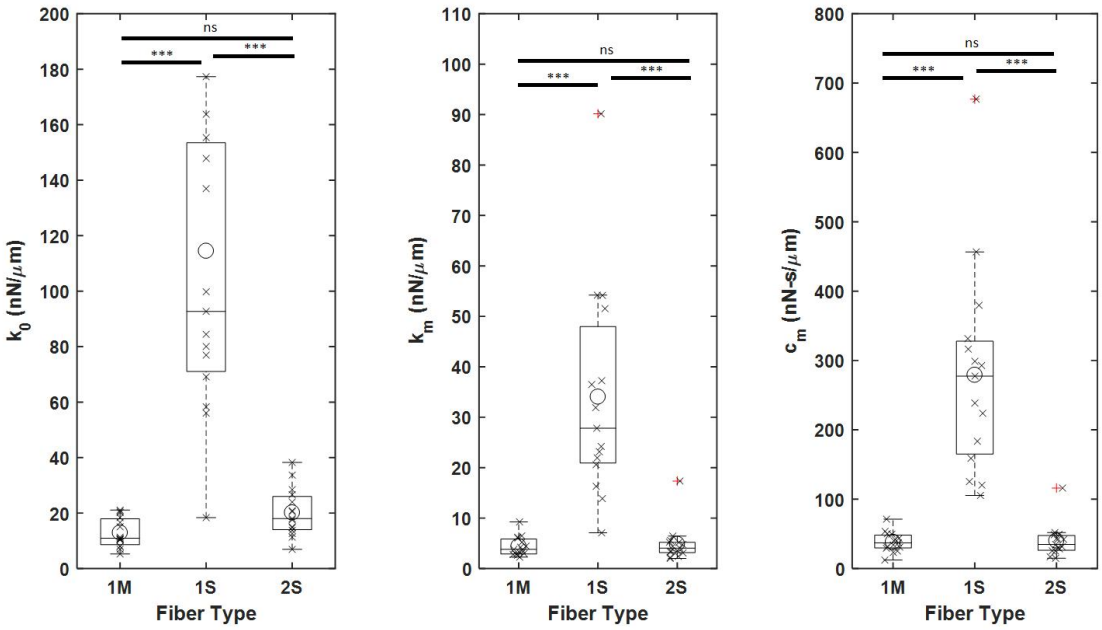

Figure 24. Spring constants and damping coefficients measurements of hMSCs of experiment group B based on forces measurements from first pulling, middle fiber (1M), first pulling, side fiber (1S), second pulling, side fiber (2S) (n = 15).

If the cell is fully separated by the middle fiber, the measurements from the side fiber (1S and 1M) during both the first and second pulling should reflect the viscoelastic properties of the cell region between the middle fiber and the side fiber. However, the results show that the side fiber measurements from the first pulling (1S) are significantly larger than those from the second pulling (2S). This confirms that the cell cannot be treated as two separate parts when it is on three fibers. The two parts segmented by the middle fiber are interactive. Interestingly, the viscoelastic property measurements from the middle fiber during the first pulling are similar to those from the side fiber during the second pulling. This similarity indicates that the viscoelastic property measurements depend on the pulling position.

Future Directions:

In this paper, we have presented a new fiber-based force measurement system capable of determining the viscoelastic response of cells repeatably. We have tested our system with hMSCs and BJ-5TA, which are relatively large cells and can exert large force to ECM compared to smaller cells including HeLa cells. It would be interesting to scale down our system by reducing the fiber spacing and fiber diameter in order to investigate the cell viscoelastic properties of smaller cells. We also proved that the cells spread on three parallel fibers cannot be treated as two independent SLS model in series. For cells which were seeded on more than 2 fibers, another mechanical model may be required to modify them. Based on our 3-fiber cell pulling case measurements, this mechanical model may be non-linear, and may need to be resolved by numerical methods. Our NFM is also capable of culturing cells under a various number of drug treatments [32]. Conducting drug treatment experiments with our system may help us to better understand how strengthening, inhibiting, or stabilizing cell cytoskeleton components including actin stress fibers, microtubules, and intermediate filaments will affect cell viscoelasticity. Last but not the least, NFM with OI approach provides us capability of measuring cell forces while giving force excitations to the cell at the same time. Studies of cell responses to certain types of mechanical stimulation may also be conducted using our system.

Conclusion:

With the previously developed NFM, we are able to investigate single living cell's viscoelastic properties by giving a step force excitation to the cell and fitting the cell force measurements to the SLS model. In cases which cells are seeded on two fibers, we tested hMSCs and BJ-5TA cells, and the viscoelastic components measurements k_0, k_m, and c_m are 26.16 ± 3.38 nN/μm, 5.81 ± 0.81 nN/μm, and 41.15 ± 5.97 nN-s/μm respectively for hMSCs, while the k_0, k_m, and c_m, measurements of BJ-5TA cells are 20.02 ± 2.89 nN/μm, 4.62 ± 0.75 nN/μm, and 45.46 ± 6.00 nN-s/μm respectively. There is no statistical difference between the two types of cells regardless of their different size and cell forces. In the cases in which cells are seeded on three fibers, we did two groups of experiments. In experiment group A, the viscoelastic measurements of the two parts of the cell body divided by the middle fiber are significantly different, while the second pulling 2 hours after the first pulling on the same fiber with the same direction yields similar measurements as the first pulling. These results indicate that the viscoelastic measurements of cells on three fibers may depend on the pulling position and proved that the cells recover 2 hours after the previous excitation. In experiment group B, two rounds of pulling are given to different fibers and the viscoelastic property measurements of the same region are significantly different between two rounds of excitation. The results from group B experiments proved that the viscoelastic property measurements of cells on three fibers depends on the excitation position. The cell body cannot be treated as two independent SLS model in series. A non-linear model may be required to describe the 3-fiber case and numerical method may be needed to resolve the system. Conducting drug studies, scaling down the system to investigate the mechanical properties of smaller cells, and providing other mechanical stimulations to single cells may be achieved in the future by our system. Overall, our new fiber-based force measurement system shows capability of measuring the viscoelastic properties of cells repeatably in single cell scale.

References:

[1] A. F. Pegoraro, P. Janmey, and D. A. Weitz, "Mechanical properties of the cytoskeleton and cells," *Cold Spring Harbor Perspectives in Biology*, vol. 9, no. 11, 2017, doi: 10.1101/cshperspect.a022038.

[2] E. H. Barriga and R. Mayor, "Adjustable viscoelasticity allows for efficient collective cell migration," *Seminars in Cell and Developmental Biology*, vol. 93. 2019. doi: 10.1016/j.semcdb.2018.05.027.

[3] B. Corominas-Murtra and N. I. Petridou, "Viscoelastic Networks: Forming Cells and Tissues," *Frontiers in Physics*, vol. 9, Jun. 2021, doi: 10.3389/fphy.2021.666916.

[4] D. A. Fletcher and R. D. Mullins, "Cell mechanics and the cytoskeleton," *Nature*, vol. 463, no. 7280. 2010. doi: 10.1038/nature08908.

[5] S. Shamipour, S. Caballero-Mancebo, and C. P. Heisenberg, "Cytoplasm's Got Moves," *Developmental Cell*, vol. 56, no. 2. 2021. doi: 10.1016/j.devcel.2020.12.002.

[6] W. TRICKEY, T. VAIL, and F. GUILAK, "The role of the cytoskeleton in the viscoelastic properties of human articular chondrocytes," *Journal of Orthopaedic Research*, vol. 22, no. 1, 2004, doi: 10.1016/s0736-0266(03)00150-5.

[7] D. T. N. Chen, Q. Wen, P. A. Janmey, J. C. Crocker, and A. G. Yodh, "Rheology of soft materials," *Annual Review of Condensed Matter Physics*, vol. 1, 2010, doi: 10.1146/annurev-conmatphys-070909-104120.

[8] B. Fabry, G. N. Maksym, J. P. Butler, M. Glogauer, D. Navajas, and J. J. Fredberg, "Scaling the microrheology of living cells," *Physical Review Letters*, vol. 87, no. 14, 2001, doi: 10.1103/PhysRevLett.87.148102.

[9] L. Blanchoin, R. Boujemaa-Paterski, C. Sykes, and J. Plastino, "Actin dynamics, architecture, and mechanics in cell motility," *Physiological Reviews*, vol. 94, no. 1, 2014, doi: 10.1152/physrev.00018.2013.

[10] N. Bonakdar *et al.*, "Mechanical plasticity of cells," *Nature Materials*, vol. 15, no. 10, 2016, doi: 10.1038/nmat4689.

[11] J. Guck *et al.*, "Optical deformability as an inherent cell marker for testing malignant transformation and metastatic competence," *Biophysical Journal*, vol. 88, no. 5, 2005, doi: 10.1529/biophysj.104.045476.

[12] D. Shin and K. Athanasiou, "Cytoindentation for obtaining cell biomechanical properties," *Journal of Orthopaedic Research*, vol. 17, no. 6, 1999, doi: 10.1002/jor.1100170613.

[13] M. Lekka *et al.*, "Cancer cell detection in tissue sections using AFM," *Archives of Biochemistry and Biophysics*, vol. 518, no. 2, 2012, doi: 10.1016/j.abb.2011.12.013.

[14] Q. Guo, S. Park, and H. Ma, "Microfluidic micropipette aspiration for measuring the deformability of single cells," *Lab on a Chip*, vol. 12, no. 15, 2012, doi: 10.1039/c2lc40205j.

[15] V. Swaminathan, K. Mythreye, E. T. O'Brien, A. Berchuck, G. C. Blobe, and R. Superfine, "Mechanical Stiffness grades metastatic potential in patient tumor cells and in cancer cell lines," *Cancer Research*, vol. 71, no. 15, 2011, doi: 10.1158/0008-5472.CAN-11-0247.

[16] K. Burton and D. L. Taylor, "Traction forces of cytokinesis measured with optically modified elastic substrata," *Nature*, vol. 385, no. 6615, 1997, doi: 10.1038/385450a0.

[17] V. Peschetola *et al.*, "Time-dependent traction force microscopy for cancer cells as a measure of invasiveness," *Cytoskeleton*, vol. 70, no. 4, 2013, doi: 10.1002/cm.21100.

[18] A. D. Powers, B. Liu, A. G. Lee, and S. P. Palecek, "Macroporous hydrogel micropillars for quantifying Met kinase activity in cancer cell lysates," *Analyst*, vol. 137, no. 17, 2012, doi: 10.1039/c2an35464k.

[19] Y. Bu, L. Li, C. Yang, R. Li, and J. Wang, "Measuring Viscoelastic Properties of Living Cells," *Acta Mechanica Solida Sinica*, vol. 32, no. 5, 2019, doi: 10.1007/s10338-019-00113-7.

[20] K. D. Webster, A. Crow, and D. A. Fletcher, "An AFM-based stiffness clamp for dynamic control of rigidity," *PLoS ONE*, vol. 6, no. 3, 2011, doi: 10.1371/journal.pone.0017807.

[21] S. C. W. Tan, W. X. Pan, G. Ma, N. Cai, K. W. Leong, and K. Liao, "Viscoelastic behaviour of human mesenchymal stem cells," *BMC Cell Biology*, vol. 9, 2008, doi: 10.1186/1471-2121-9-40.

[22] R. M. Hochmuth, “Micropipette aspiration of living cells,” *Journal of Biomechanics*, vol. 33, no. 1, pp. 15–22, Jan. 2000, doi: 10.1016/S0021-9290(99)00175-X.

[23] A. D. Doyle, F. W. Wang, K. Matsumoto, and K. M. Yamada, “One-dimensional topography underlies three-dimensional fi brillar cell migration,” *Journal of Cell Biology*, vol. 184, no. 4, 2009, doi: 10.1083/jcb.200810041.

[24] S. P. Carey, C. M. Kraning-Rush, R. M. Williams, and C. A. Reinhart-King, “Biophysical control of invasive tumor cell behavior by extracellular matrix microarchitecture,” *Biomaterials*, vol. 33, no. 16, 2012, doi: 10.1016/j.biomaterials.2012.02.029.

[25] P. Friedl and K. Wolf, “Plasticity of cell migration: A multiscale tuning model,” *Journal of Cell Biology*, vol. 188, no. 1. 2010. doi: 10.1083/jcb.200909003.

[26] B. A. C. Harley, H. do Kim, M. H. Zaman, I. v Yannas, D. A. Lauffenburger, and L. J. Gibson, “Microarchitecture of three-dimensional scaffolds influences cell migration behavior via junction interactions,” *Biophysical Journal*, vol. 95, no. 8, 2008, doi: 10.1529/biophysj.107.122598.

[27] K. Sheets, J. Wang, W. Zhao, R. Kapania, and A. S. Nain, “Nanonet Force Microscopy for Measuring Cell Forces,” *Biophysical Journal*, vol. 111, no. 1, 2016, doi: 10.1016/j.bpj.2016.05.031.

[28] A. Hall *et al.*, “Nanonet force microscopy for measuring forces in single smooth muscle cells of the human aorta,” *Molecular Biology of the Cell*, vol. 28, no. 14, 2017, doi: 10.1091/mbc.E17-01-0053.

[29] A. Padhi *et al.*, “Force-exerting perpendicular lateral protrusions in fibroblastic cell contraction,” *Communications Biology*, vol. 3, no. 1, 2020, doi: 10.1038/s42003-020-01117-7.

[30] J. M. Szulczewski, D. R. Inman, M. Proestaki, J. Notbohm, B. M. Burkel, and S. M. Ponik, “Directional cues in the tumor microenvironment due to cell contraction against aligned collagen fibers,” *Acta Biomaterialia*, vol. 129, 2021, doi: 10.1016/j.actbio.2021.04.053.

[31] A. Jana, I. Nookaew, J. Singh, B. Behkam, A. T. Franco, and A. S. Nain, “Crosshatch nanofiber networks of tunable interfiber spacing induce plasticity in cell migration and

cytoskeletal response," *FASEB Journal*, vol. 33, no. 10, 2019, doi: 10.1096/fj.201900131R.

[32] P. Sharma *et al.*, "Aligned and suspended fiber force probes for drug testing at single cell resolution," *Biofabrication*, vol. 6, no. 4, 2014, doi: 10.1088/1758-5082/6/4/045006.

Appendix A: Cell area before and after the cell pulling plots

Two-fiber cases

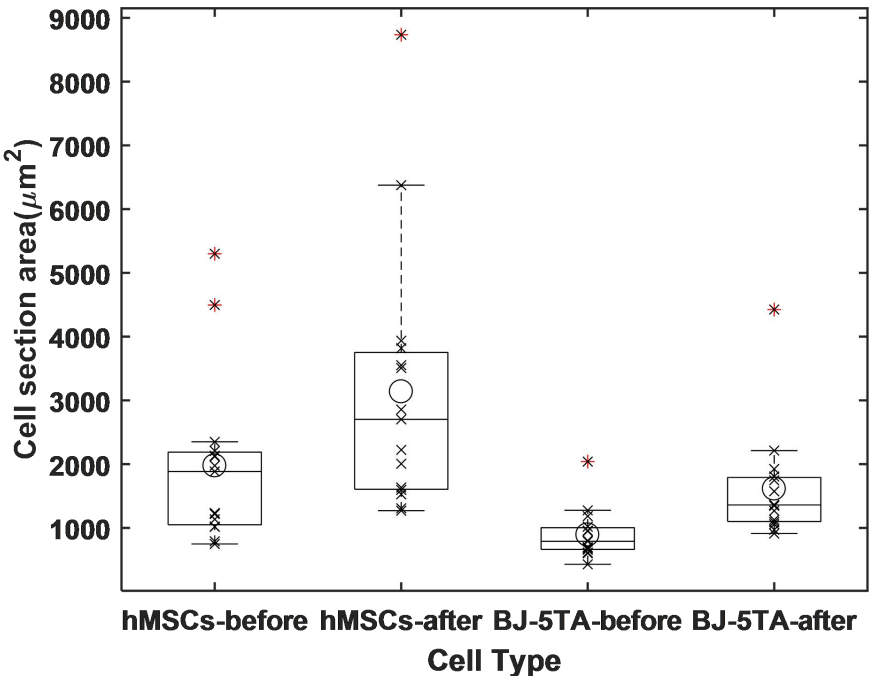

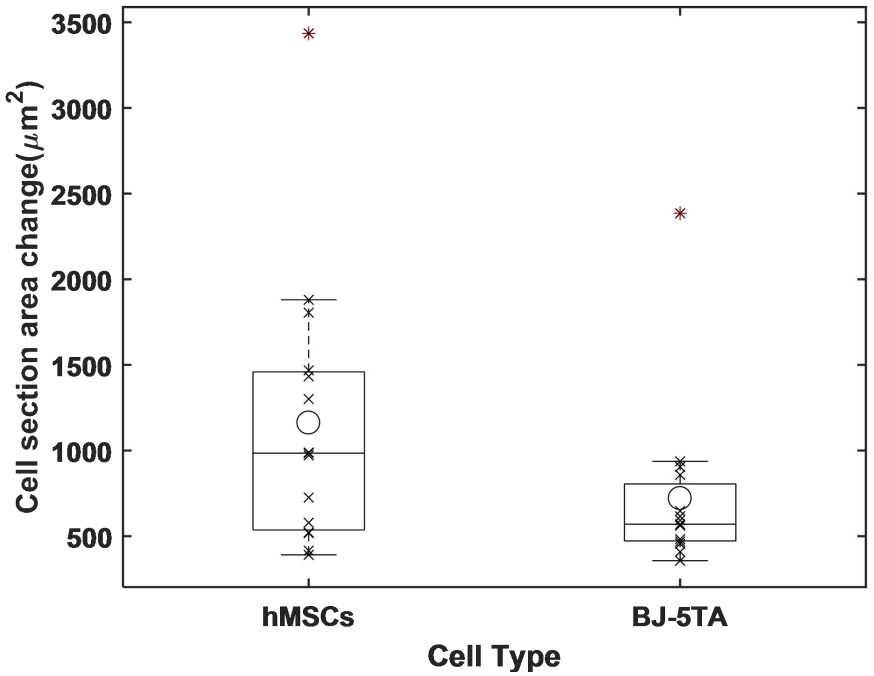

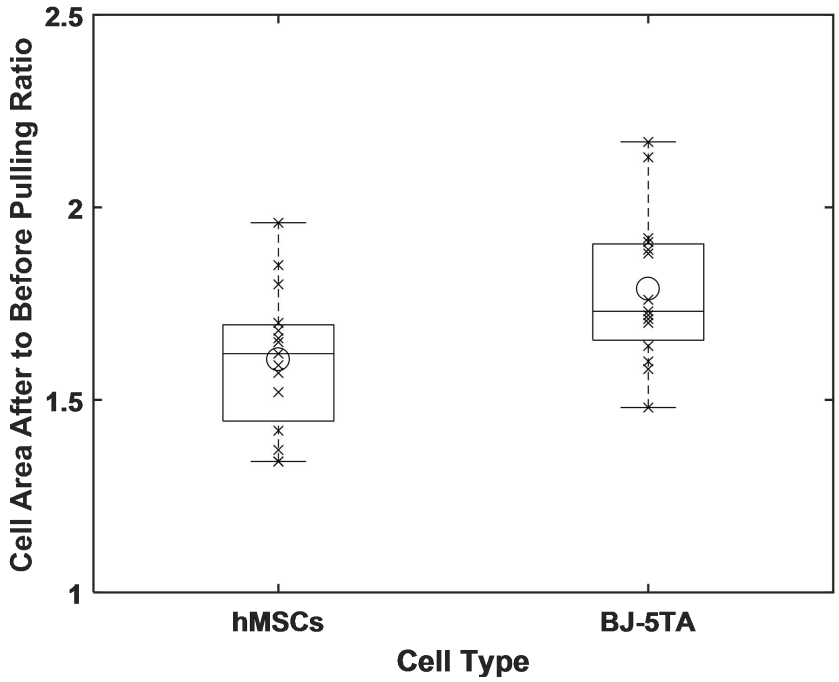

Three-fiber cases group A

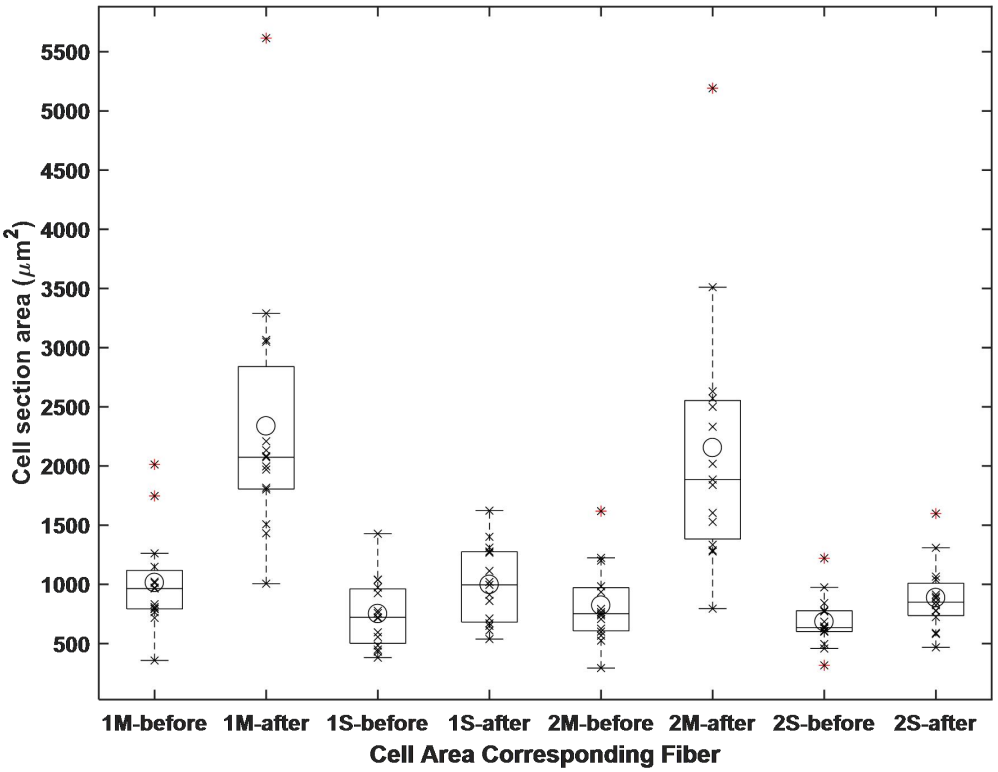

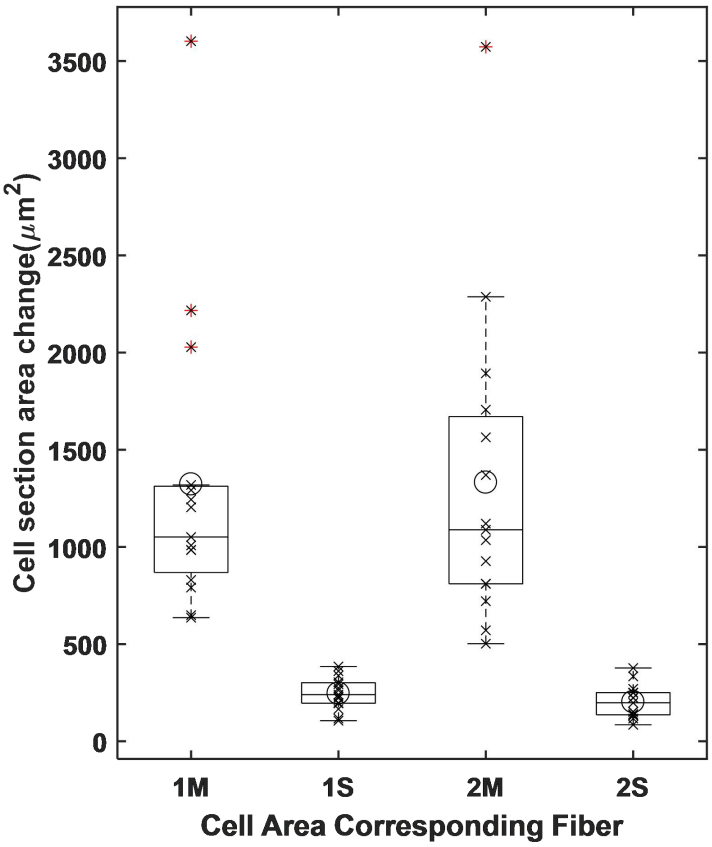
Cell section area change(μm^2)
3500
3000
2500
2000
1500
1000
500
0
1M
1S
2M
2S
Cell Area Corresponding Fiber

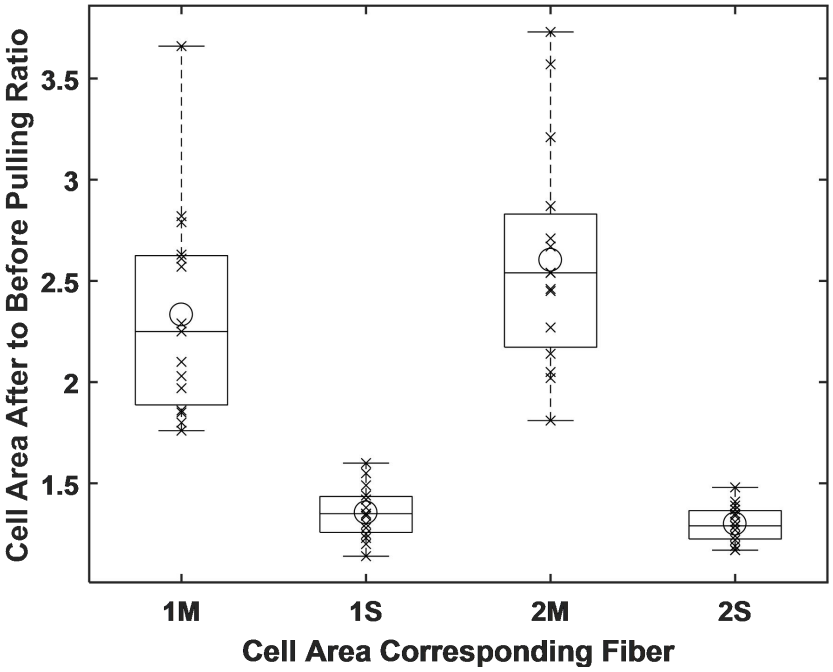
Cell Area After to Before Pulling Ratio
3.5
3
2.5
2
1.5
1M
1S
2M
2S
Cell Area Corresponding Fiber

Three-fiber cases group B

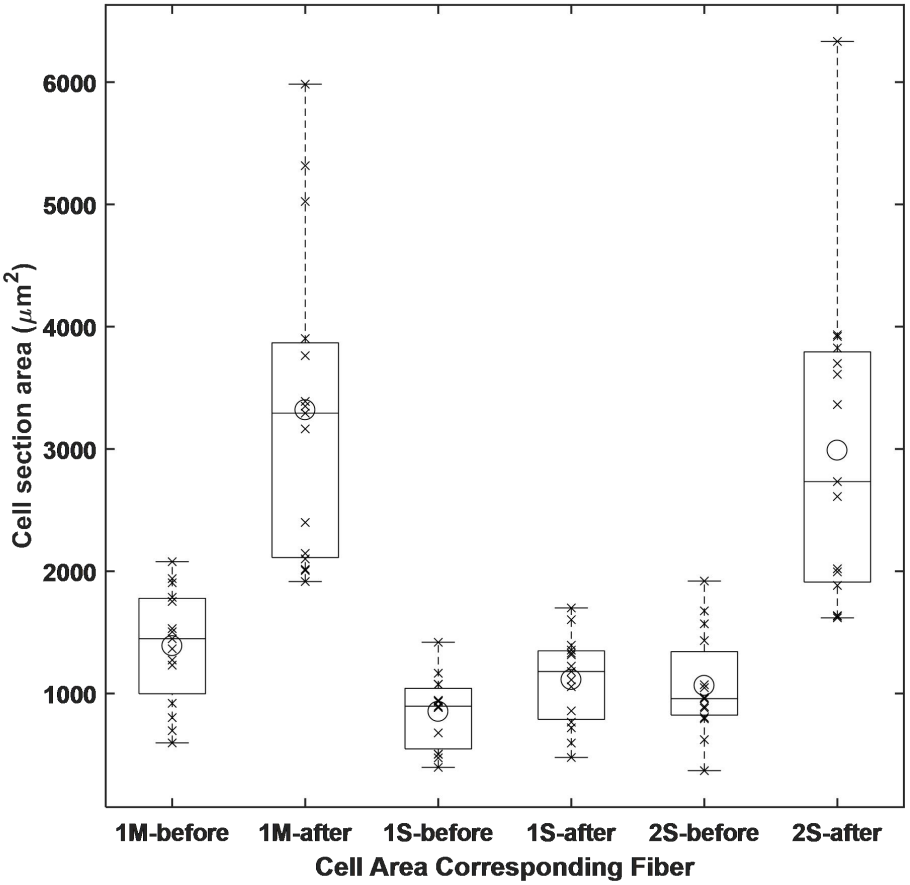

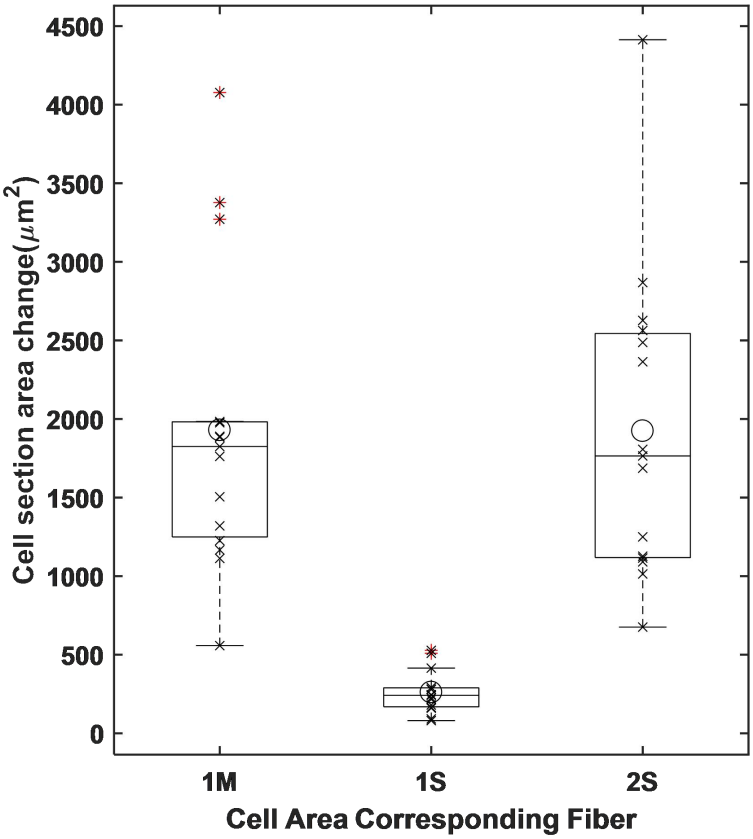
4500
4000
3500
3000
2500
2000
1500
1000
500
0
Cell section area change(μm^2)
1M
1S
2S
Cell Area Corresponding Fiber

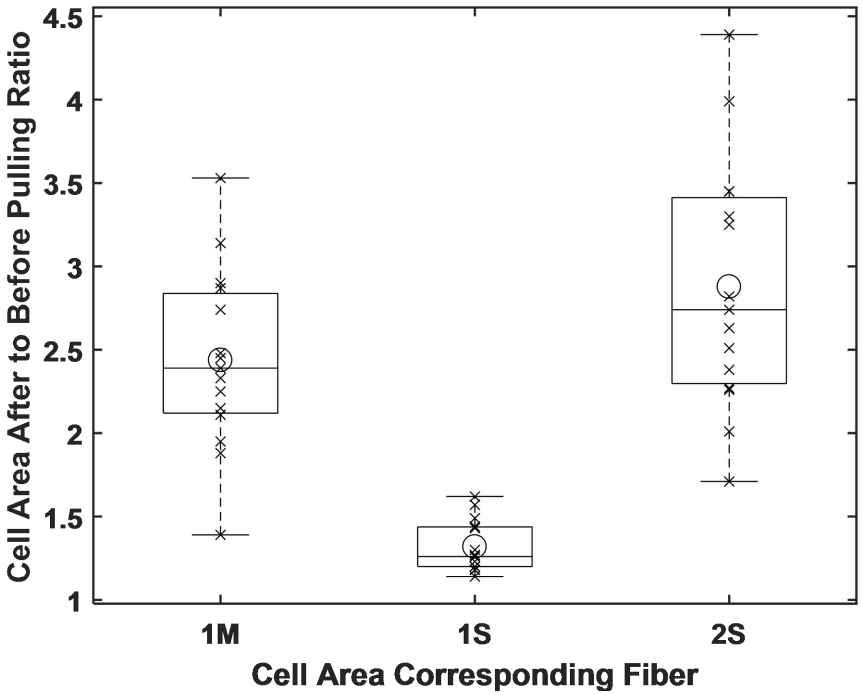
4.5
4
3.5
3
2.5
2
1.5
1
Cell Area After to Before Pulling Ratio
1M
1S
2S
Cell Area Corresponding Fiber

Three-fiber cases cell area ratio before pulling

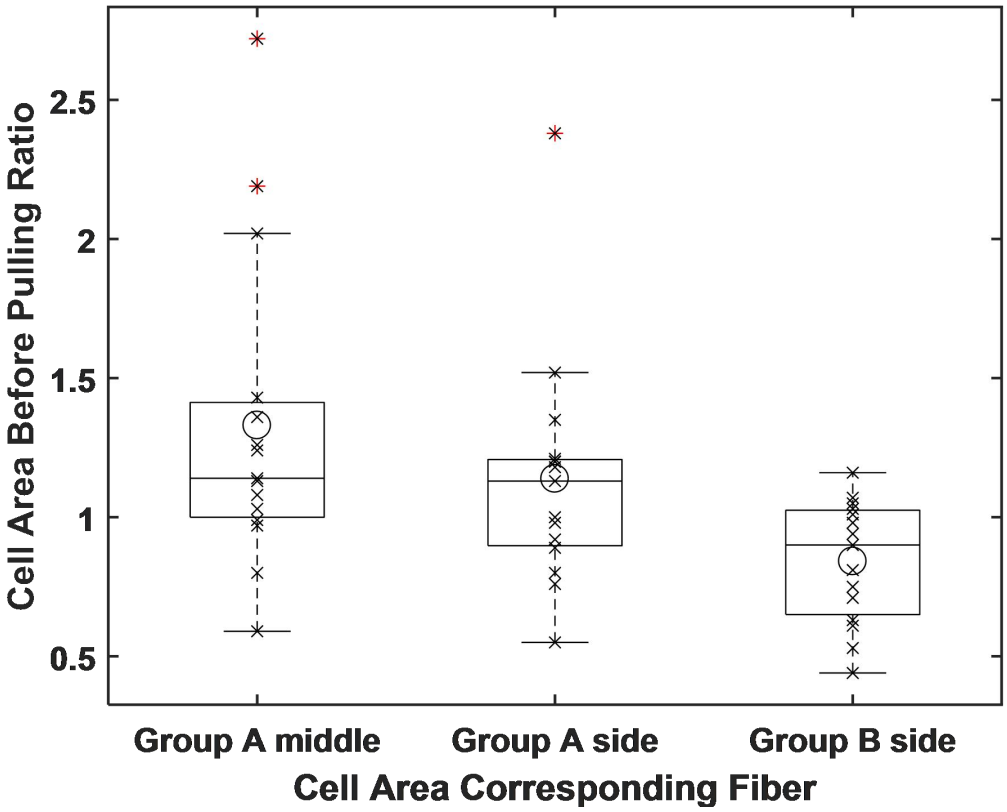

Appendix B: Area increases (before to after) pulling vs. cell viscoelastic measurements

Three-fiber case group A 1st pulling middle fiber

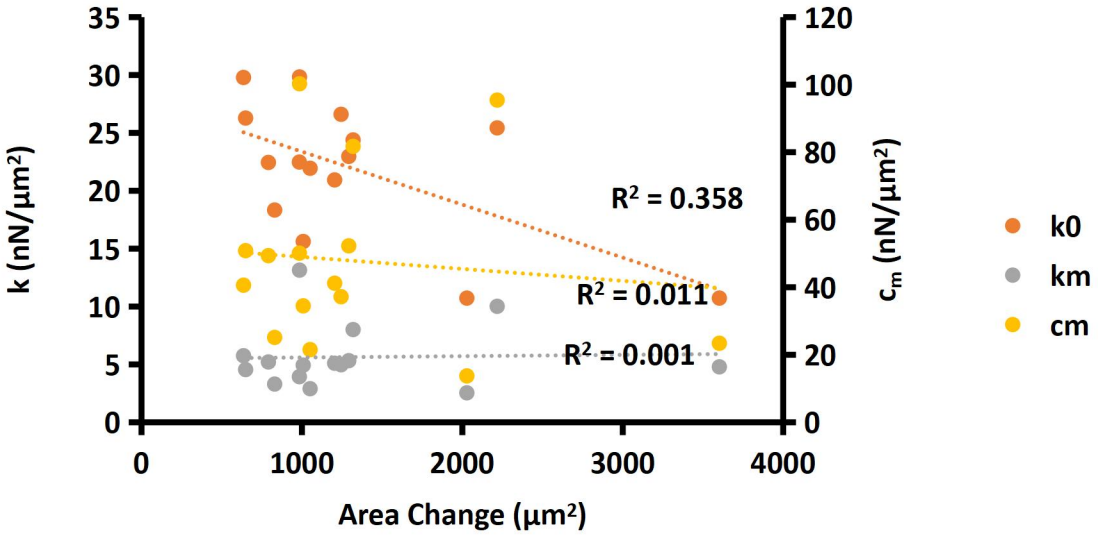

Three-fiber case group A 1st pulling side fiber

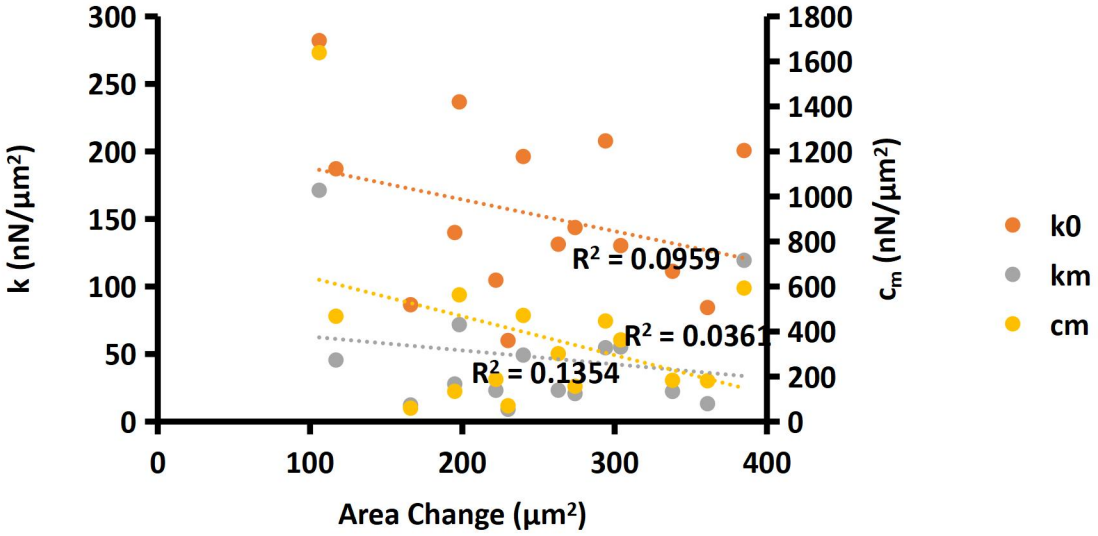

Three-fiber case group A 2nd pulling middle fiber

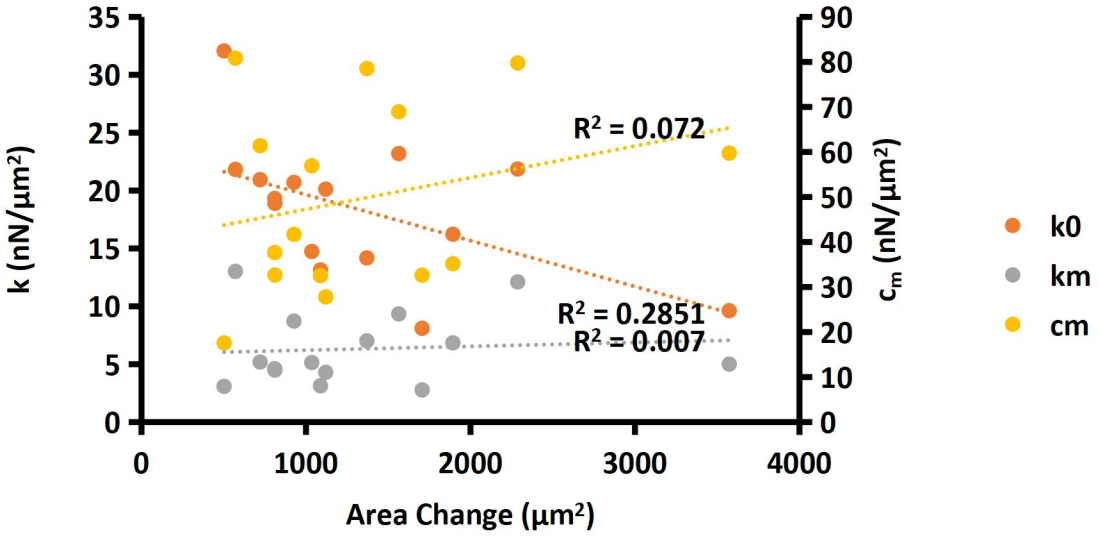

Three-fiber case group A 2nd pulling side fiber

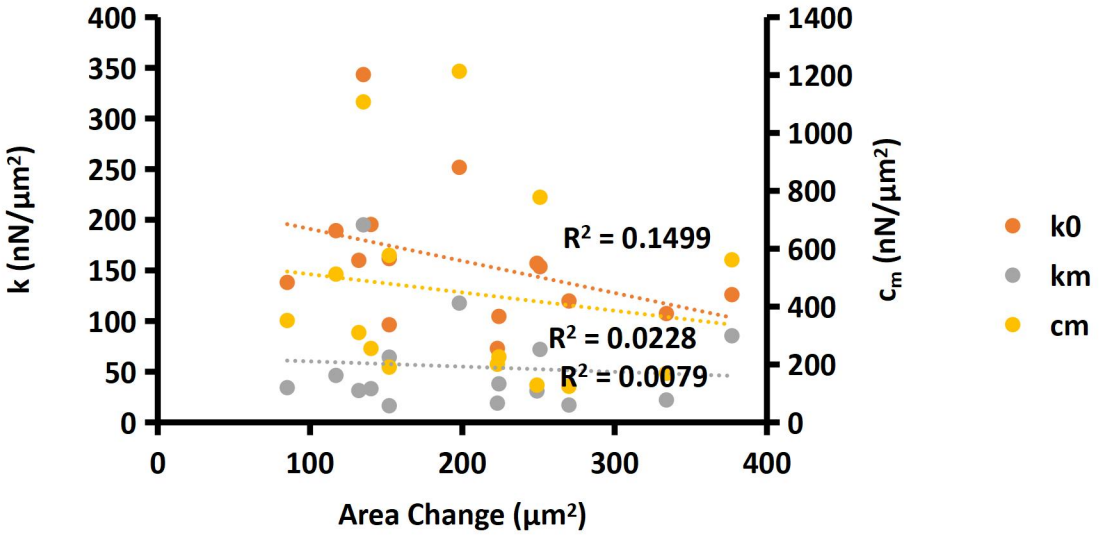

Three-fiber case group B 1st pulling middle fiber

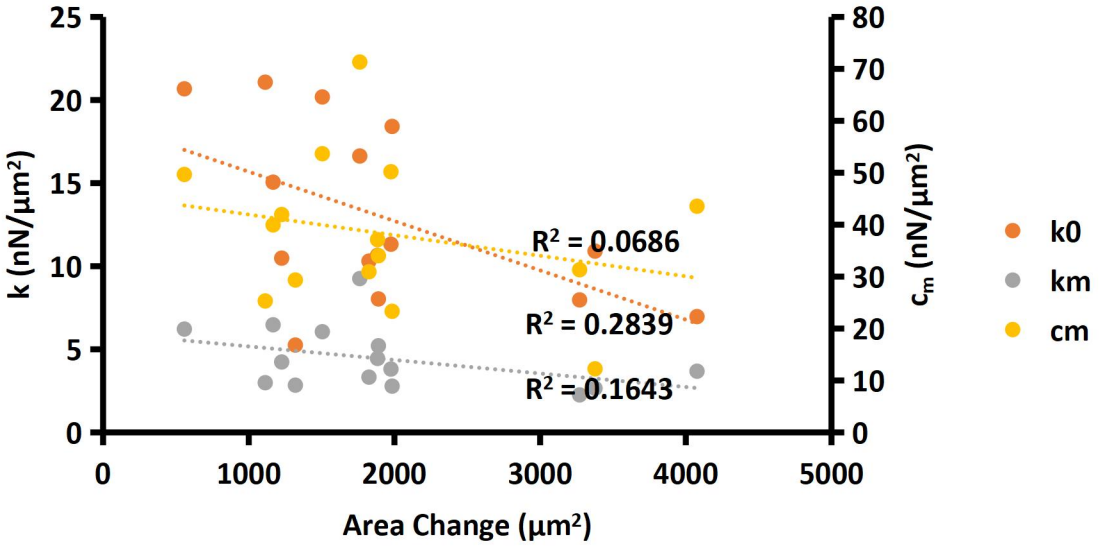

Three-fiber case group B 1st pulling side fiber

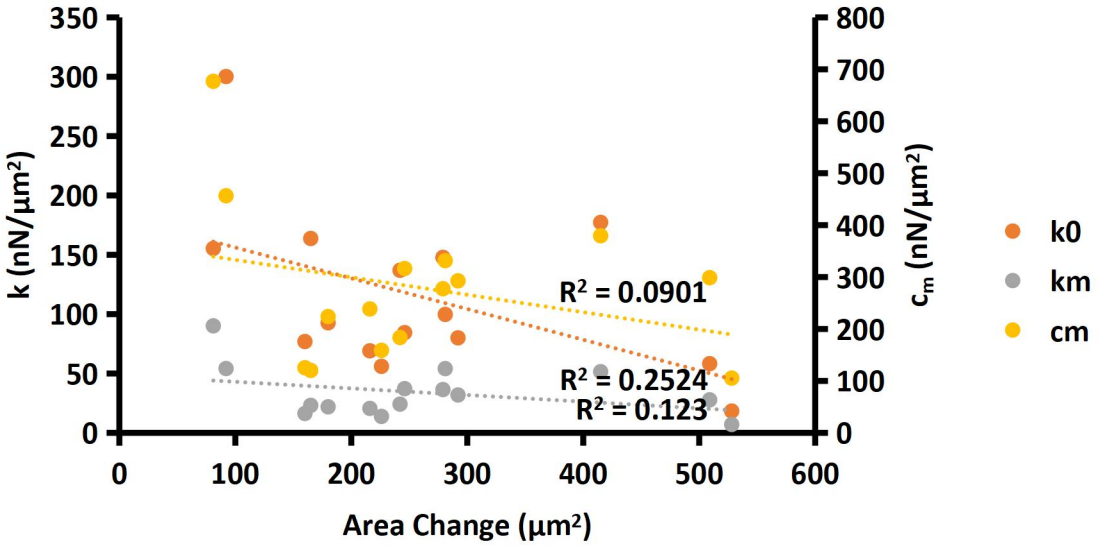

Three-fiber case group B 2nd pulling middle fiber

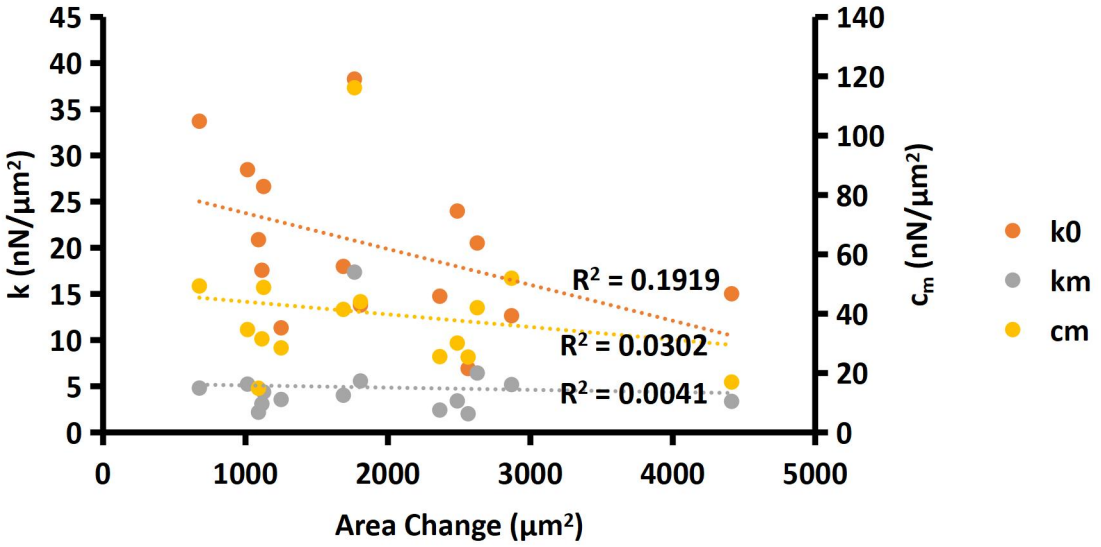

Appendix C: Area increases ratio (after to before) pulling vs. cell viscoelastic measurements

Two-fiber case hMSCs

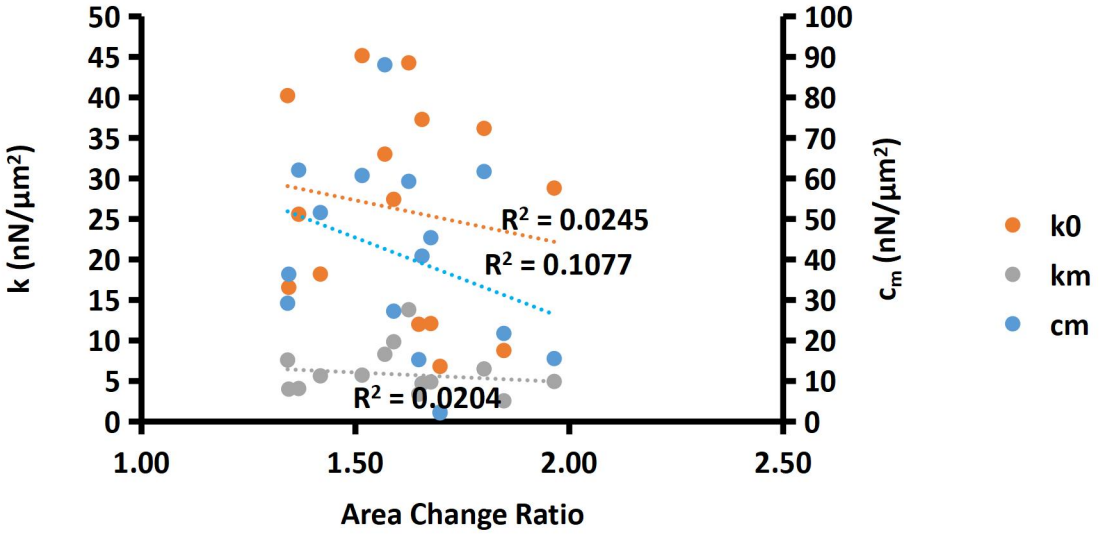

Two-fiber case BJ-5TA cells

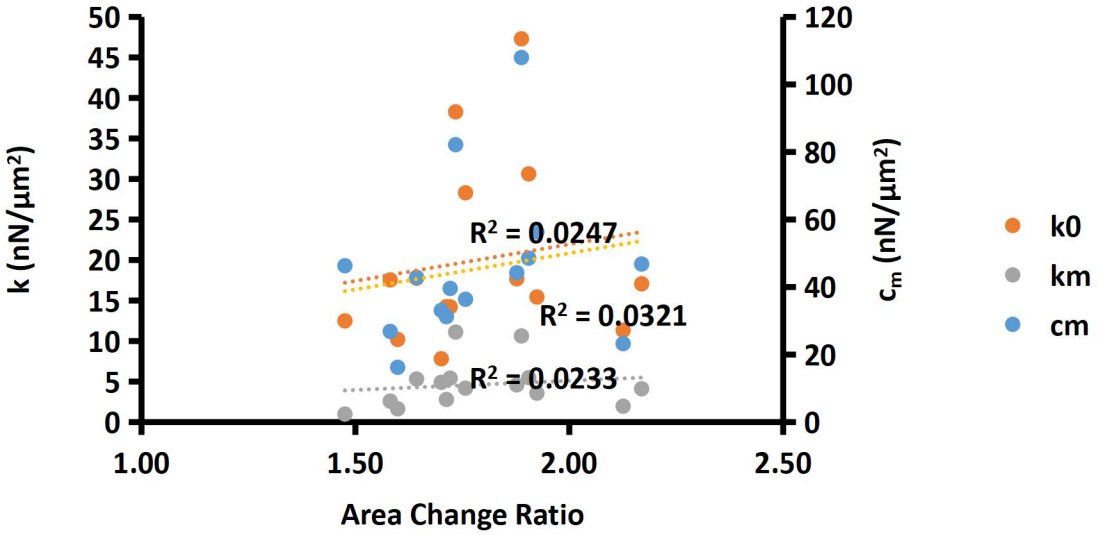

Three-fiber case group A 1st pulling middle fiber

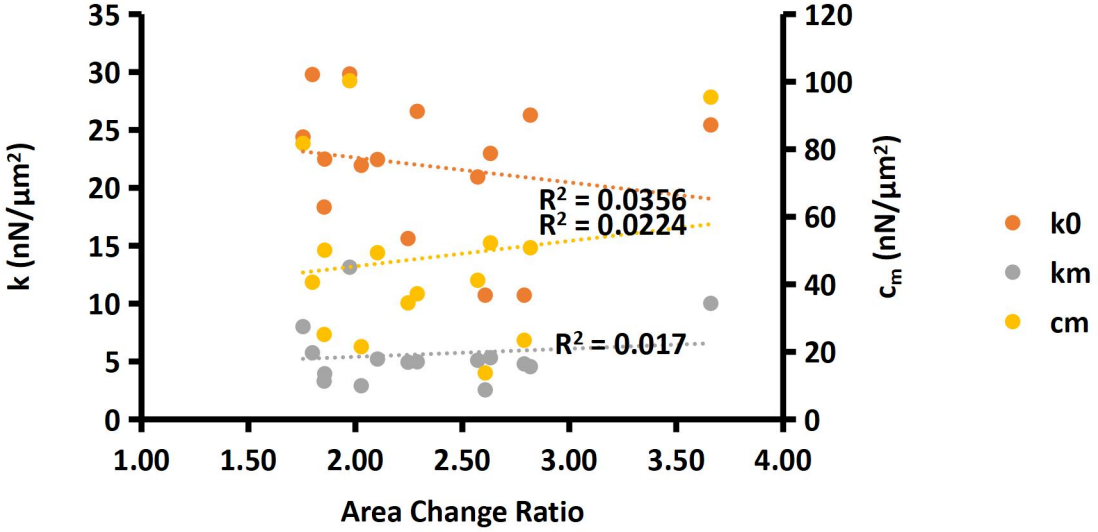

Three-fiber case group A 1st pulling side fiber

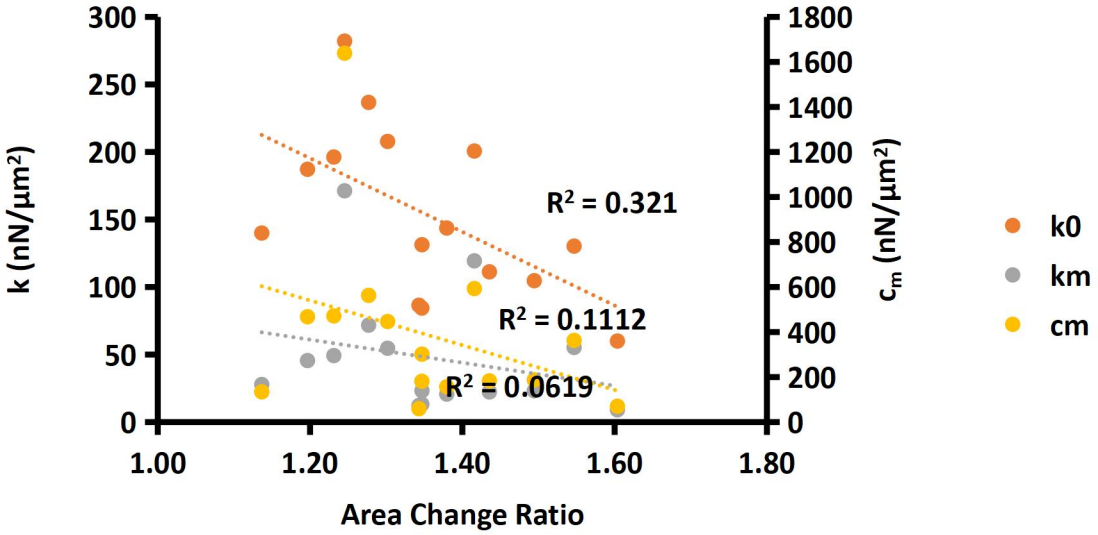

Three-fiber case group A 2nd pulling middle fiber

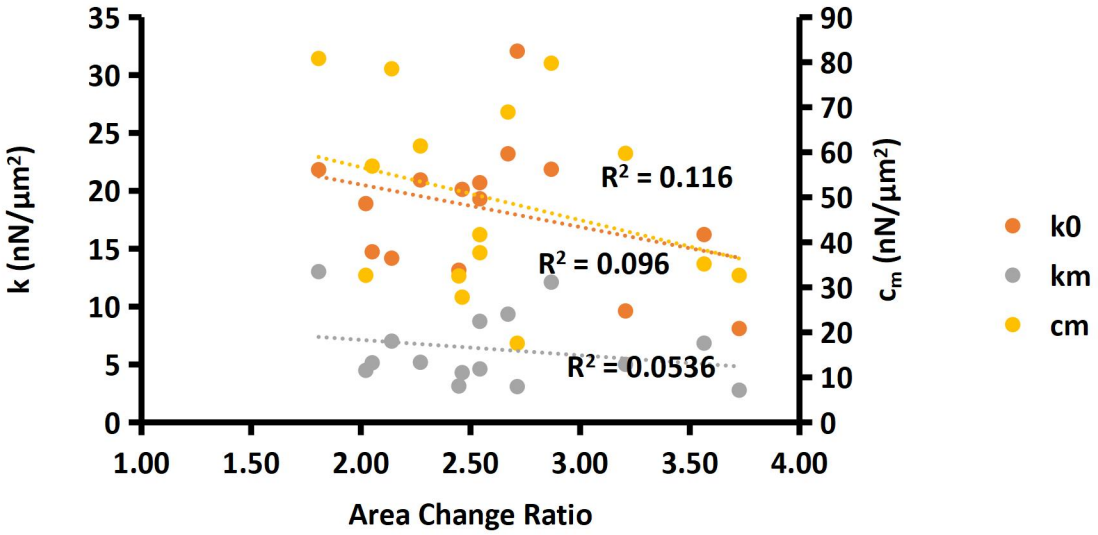

Three-fiber case group A 2nd pulling side fiber

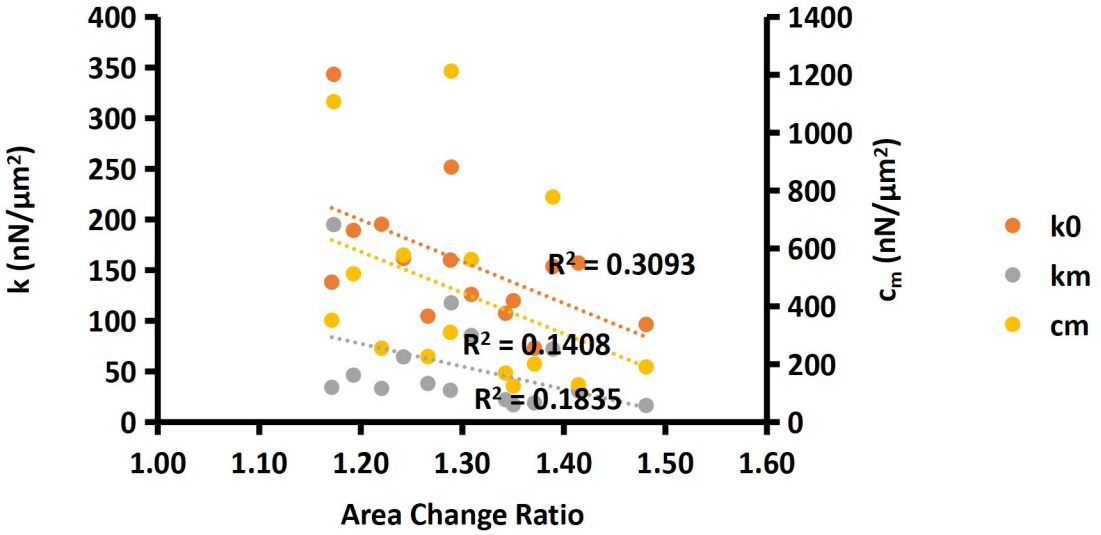

Three-fiber case group B 1st pulling middle fiber

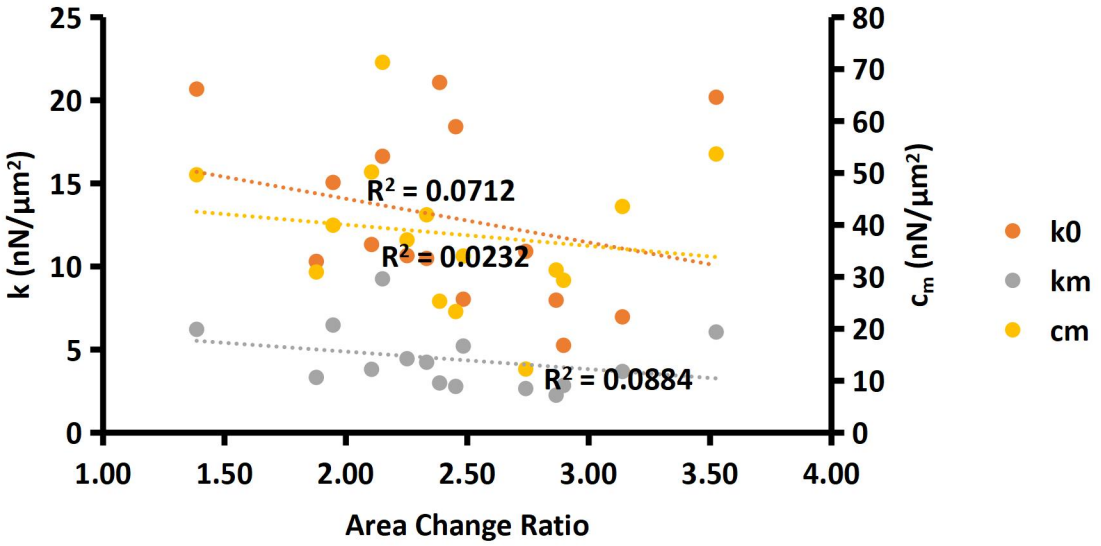

Three-fiber case group B 1st pulling side fiber

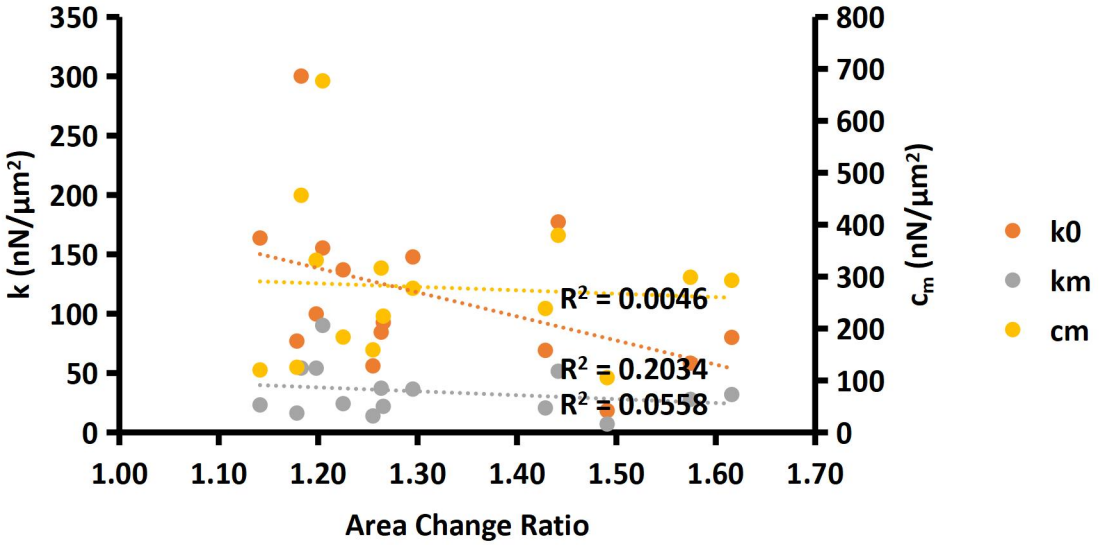

Three-fiber case group B 2nd pulling side fiber

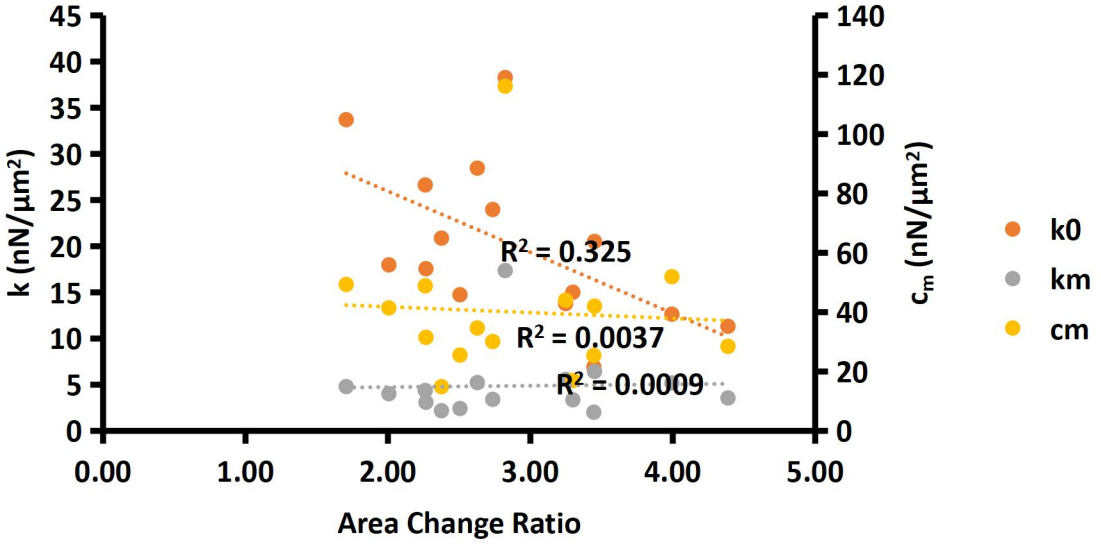

Appendix D: Fluorescent images examples

hMSCs (Red: actin filaments, Blue: chromosome, Green: paxillin)

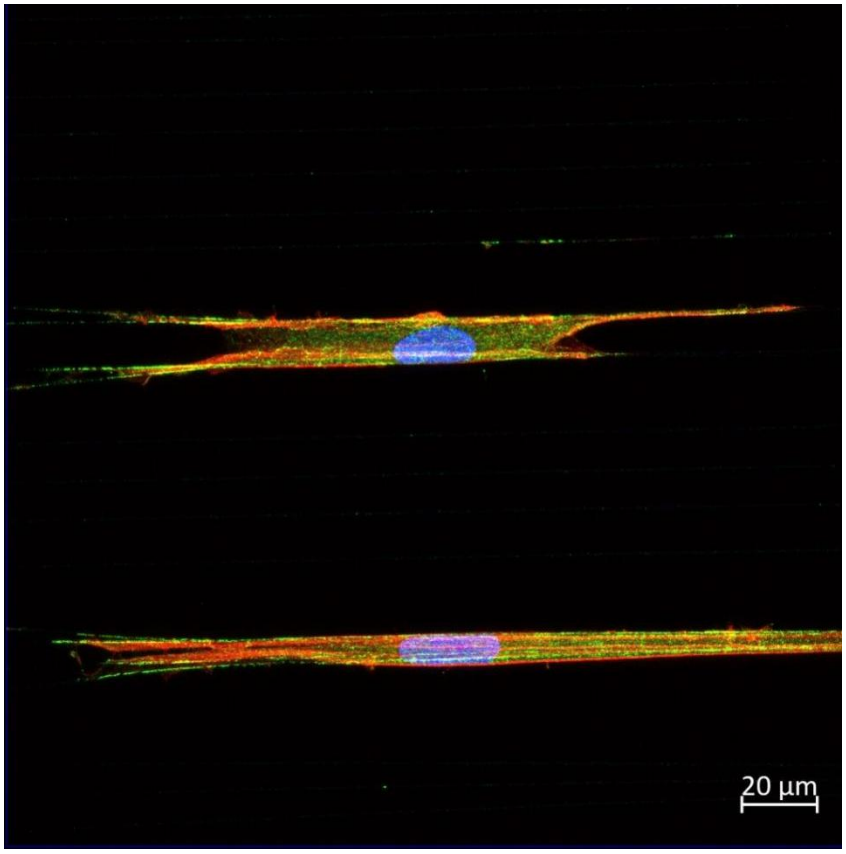

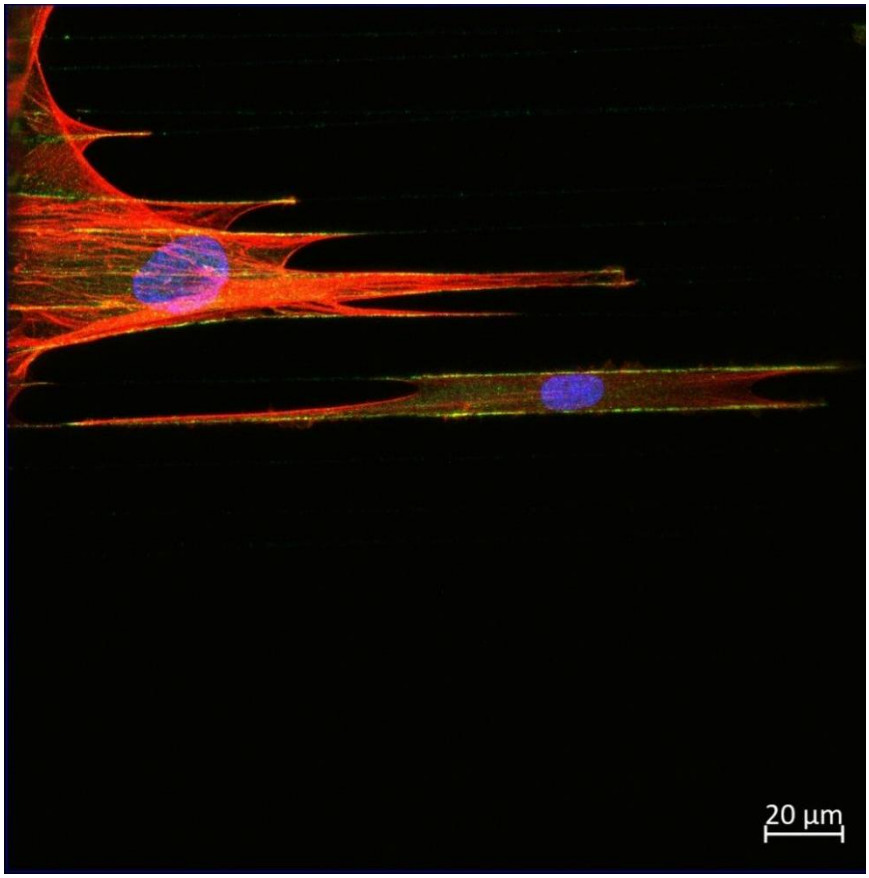
20 µm

BJ-5TA cells (Red: actin filaments, Blue: chromosome, Green: paxillin)

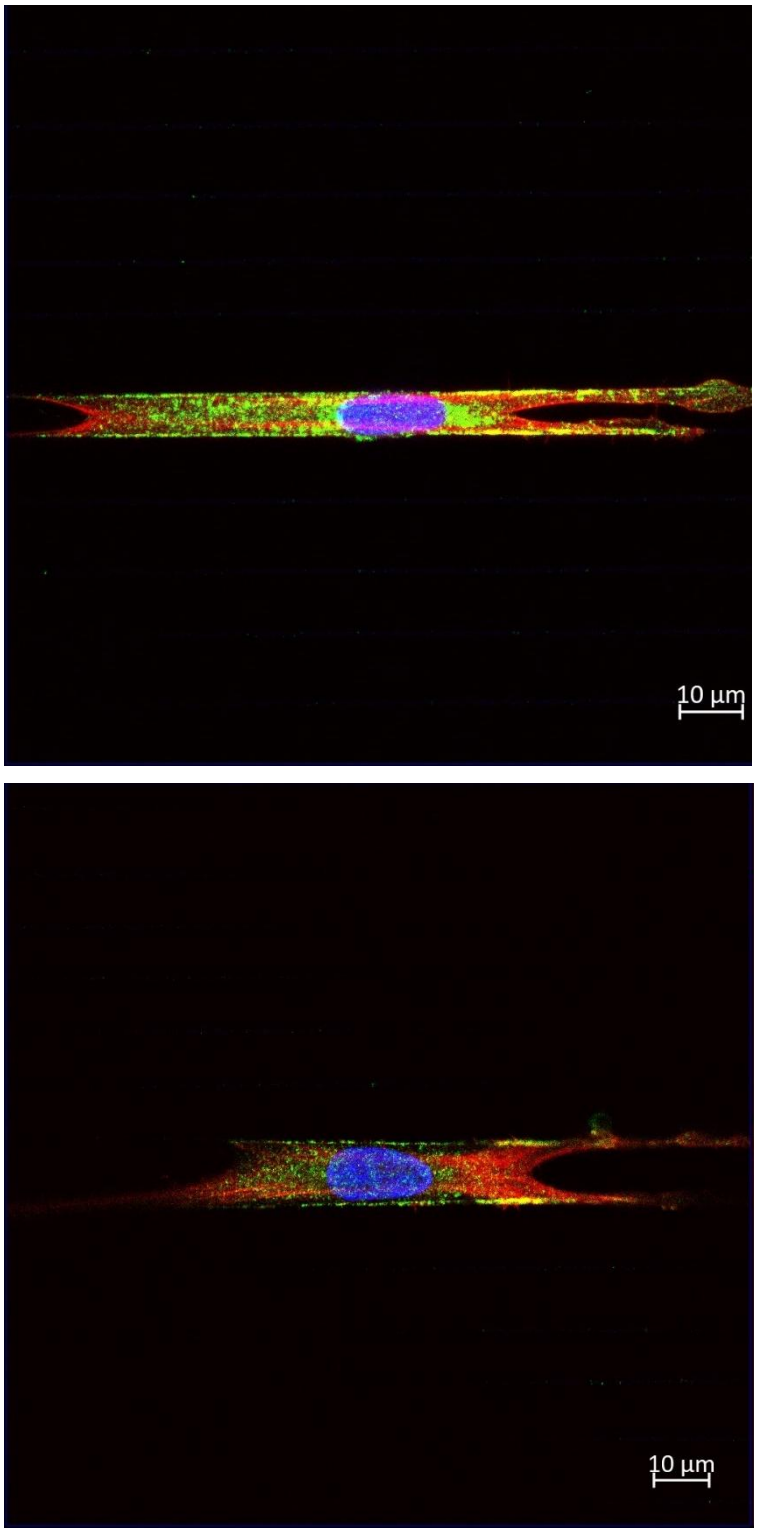

Appendix E: Nucleus and cell body absolute area measurements

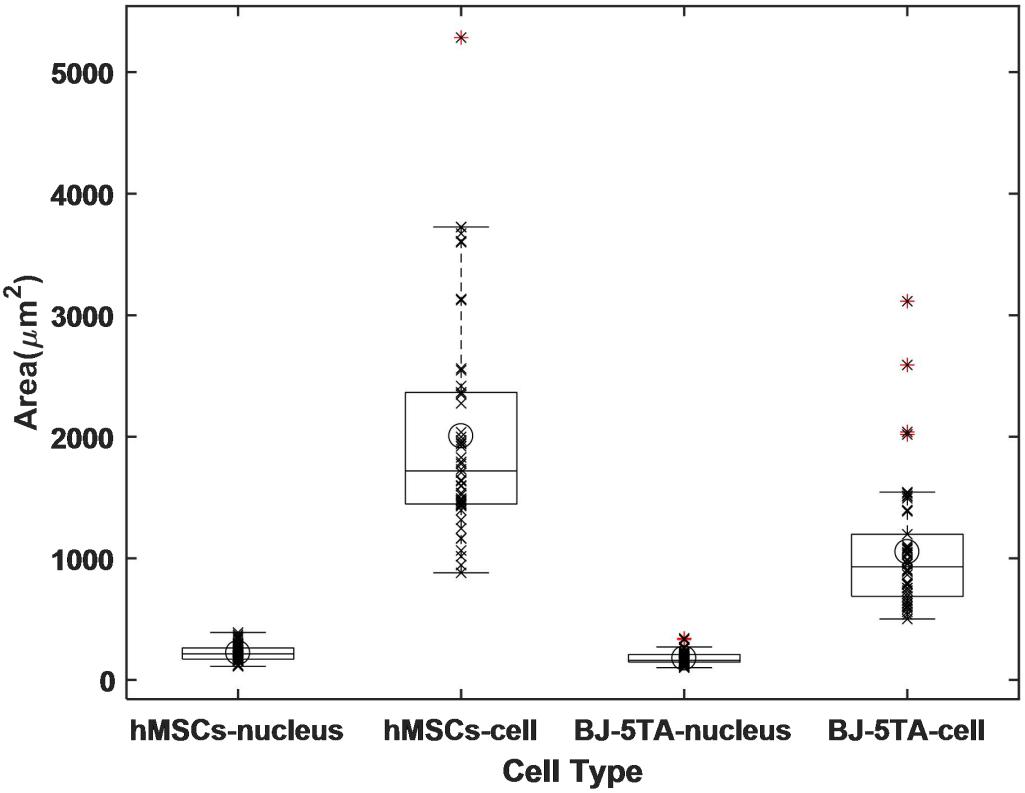

Appendix F: Modified stiffness and viscosity calculation

To convert the spring constants and damping coefficients measurements to cell size independent physical properties, the following equation which includes the cell dimensions was introduced. This calculation is similar to the conversion of young's modulus from spring constant measurements.

$$E = \frac{k \cdot W}{A} \tag{5}$$

Where E is the modified stiffness in Pa, k is the spring constant in N/m, W is the cell width in m, and A is the cell-fiber contact area in m^2.

The cell width can be measured directly from the experiment images, while the cell-fiber contact area is estimated by the following equation.

$$A = \pi \cdot D \cdot W \tag{6}$$

Where A is the cell-fiber contact area in m^2, D is the fiber diameter which is known in m, and W is the width in m.

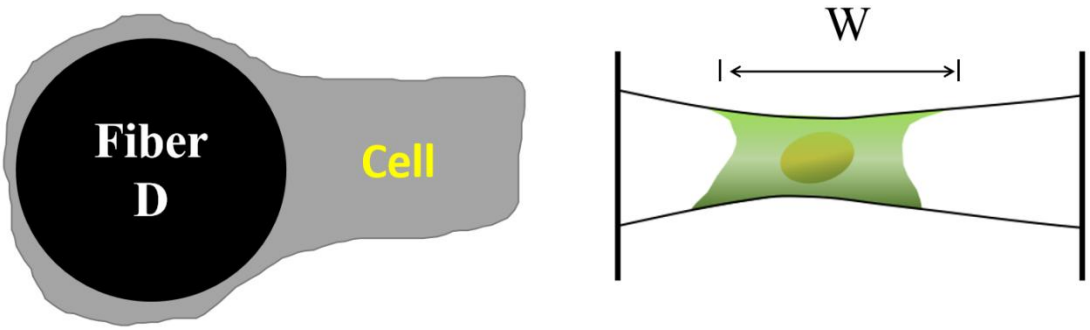

Similarly, the modified viscosity can be calculated with the following equation.

$$\mu = \frac{c \cdot W}{A} \tag{7}$$

Where μ is the modified viscosity in Pa-s, c is the damping coefficient in N-s/m, W is the cell width in m, and A is the cell-fiber contact area in m^2.